# Distribution of Oxygen Concentration inside Biofilms and Development of New Wastewater Treatment Process by Controlling Microenvironment

# 生物膜内の酸素濃度分布の解明および その制御による新規排水処理プロセスの開発

**February 2004**

早稲田大学大学院　理工学研究科

応用化学専攻　化学工学研究

**Kazuaki HIBIYA**

日比谷　和明

# Contents

## Chapter I

### GENERAL INTRODUCTION

**Nitrogen Removal from Wastewater by Biofilm Method and Research of Condition in a Biofilm**



## Chapter II

### DEVELOPMENT OF MICROELECTORDE

**Measuring Distributions of Substrate Concentration inside Biofilm by Ion-selective Microelectrodes and an Oxygen Selective Microelectrode**

# Chapter III

## SIMULATION INSIDE BIOFILM

**Simple Prediction of Oxygen Penetration Depth in Biofilms for Wastewater Treatment**



# Chapter IV

## STEP CHANGE ANALYSIS

**Observation of substrate concentration profile inside biofilm in step change analysis**

# Chapter V

## NEW NITROGEN REMOVAL SYSTEM

**Simultaneous Nitrification and Denitrification by Controlling Vertical and Horizontal Microenvironment in a Membrane-Aerated Biofilm Reactor**

## Chapter VI

### CONCLUSION AND PERSPECTIVE



## References



## Acknowledgement



## Appendix

# Chapter I

## GENERAL INTRODUCTION

**Nitrogen Removal from Wastewater by Biofilm Method and Research of Condition in a Biofilm**

## 1.1 INTRODUCTION

Nitrogen pollutants discharged from domestic and industrial wastewaters cause the eutrophication phenomena in ponds, lakes and inner bay. To obviate this problem, it is necessary to remove nitrogen compounds with a high efficiency from these wastewaters. Biological nitrogen removal is most frequently used as a low cost wastewater treatment system. However, it needs two successive processes, i.e., nitrification in aerobic condition and denitrification in anaerobic condition. Consequently, using two reactors, equipment becomes large. Thus, the introduction of a single nitrogen removal system with compact size and easy maintenance placed in small space has been strongly desired.

Here, I focus on the thick layer of cells referred to as a "biofilm" that microorganisms formed by adhering to the solid surface. Nitrogen removal could be accomplished under oxygen concentration gradients in the depth direction within the biofilm, which creats aerobic and anaerobic conditions. To attain simultaneous nitrification and denitrification, it is important to control distributions of oxygen concentration and microbial population within the biofilm. Thus, it is useful to monitor oxygen concentration and microbial population by utilizing a microelectrode, a very small needle-type sensor, and fluorescence in situ hybridization (FISH) technique directly detecting specific bacteria such as ammonia-oxidizing and nitrite-oxidizing bacteria in the biofilm without a culture operation.

In this study, taking advantage of precise control of oxygen concentration inside a biofilm, a membrane aeration biofilm reactor (MABR) in which oxygen is supplied from the inside of the porous membrane is developed. This reactor configuration could create counter diffusion of ammonia and oxygen in a biofilm, resulting in coexistence of nitrifying and denitrifying bacteria in the single biofilm. I would examine feasibility of this concept by experimental and simulation analyses, and then demonstrate that nitrification and denitrification occurs sequentially in the single reactor.

# 1.2 BACKGROUNDS

## 1.2.1 Nitrogen Removal

Nitrogenous pollutants from domestic and industrial wastewaters are responsible for promoting the eutrophication effect in ponds and lakes [1]. Thus, the removal of nitrogen compounds from wastewater is of increasing importance. Biological nitrogen removal involves two successive processes, i.e., nitrification and denitrification. Nitrification transforms ammonia to a more oxidized nitrogen compound such as nitrite or nitrate which is then converted to nitrogen gas in the subsequent denitrification process [2]. These two processes are usually carried out in different reactors because nitrification occurs under an aerobic condition while denitrification prevails in the absence of oxygen [3]. However, the two processes are complementary in many ways, i.e., 1) nitrification produces nitrite or nitrate which is a reactant in denitrification, 2) nitrification reduces the pH that is raised in denitrification, and 3) denitrification generates the alkalinity that is required in nitrification [4]. Therefore, there exist obvious advantages to performing simultaneous nitrification and denitrification in a single reactor.

Nitrification:

$$2NH_4^+ + 3O_2 \rightarrow 2NO_2^- + 2H_2O + 4H^+ \quad (1)$$

$$2NO_2^- + O_2 \rightarrow 2NO_3^- \quad (2)$$

Denitrification:

$$2NO_3^- + 2H^+ \rightarrow 2NO_2^- + 2OH^- \quad (3)$$

$$2NO_2^- + 4H^+ \rightarrow N_2 \uparrow + 2H_2O + 2OH^- \quad (4)$$

## 1.2.2 Biofilm method

There are two advantages of biological wastewater treatment using a fluidized bed reactor with a biofilm fixed on particles: 1) the reactor has active transfer phenomena accelerated by fluidizing materials, and 2) the reactor retains 5-10 times higher biomass concentration than conventional activated sludge reactors [5, 6]. This technique had been successfully applied to the removal of nutrients and harmful compounds from domestic and industrial wastewater [7-11]. In wastewater treatment using a biofilm, bacteria inside the biofilm degrade substrates that have diffused into the biofilm. In this process, a shortage of oxygen for biological oxidation is frequently observed because nominal oxygen is soluble in water. Therefore, the spatial distribution of oxygen in biofilms is very important for the operation of reactors.

### 1.2.3 Analysis inside biofilm

Currently, new methods of evaluating the physical and microbial properties of a biofilm are being developed, using a needle-type microelectrode with a tip diameter of 3-20 micrometers to measure the substrate concentration distribution in a biofilm [12]. Liquid ion-selective (LIX) microelectrodes can be applied to measure pH and the concentrations of ammonium, nitrite and nitrate ions [13]. Moreover, a fluorescent in situ hybridization (FISH) method is highly effective for analyzing complex microbial communities in a biofilm, because specific bacterial cells are detected using 16S-rRNA-targeted oligonucleotide probes labeled with a fluorescent compound [14-16]. A hybrid analysis of using with microelectrodes and the FISH method clarifies the microenvironment inside a biofilm in a rotated-disk type reactor and a fluidized bed reactor, which is important in the design of a biofilm reactor system [17, 18].

The internal physical features of biofilms and microbial distribution in biofilms have been clarified [19, 20]. By physical analysis, the structures of biofilms and substrate distributions in biofilms were measured using a confocal laser scanning microscope (CLSM) and microelectrodes [21, 22]. By microbial analysis, bacterial species and their distributions inside biofilms were determined using molecular biology techniques such as fluorescent in situ hybridization (FISH) and polymerase chain reaction (PCR) analysis followed by denaturing gradient gel electrophoresis (DGGE) [23, 24]. Moreover, biofilm characteristics were mathematically modeled taking into account of complex phenomena occurring in biofilms [25]. These extensive research studies clarified the microbial ecology inside biofilms. In particular, biofilms have distinct microbial distributions of heterotrophic bacteria and autotrophic nitrifying bacteria [26, 27]. These distributions are caused by the competition between both bacterial populations for oxygen uptake [28]. Therefore, the oxygen distribution in biofilms should be elucidated.

The internal features of biofilms differ greatly with age, thickness, density, porosity and tortuousity. In particular, the substrate and microbial distributions in biofilms change with biofilm thickness. These distributions are closely related to mass transfer phenomena [29]. In fact, the diffusion coefficient of biofilms, which is lower than that of water, is influenced by their density, porosity, pore size, convection, type of extracellular polymeric substances (EPSs) and minerals [30].

### 1.2.4 Biofilm modeling

Nutrient removal from wastewater is necessary to prevent eutrophication of the receiving waters. Fluidized bed bioreactors have been found to remove nutrients and other pollutants both from domestic and industrial wastewaters. Most of the previous works on biofilm process assumed that the reaction follows Monod-type, first order or zero order equation. Even though the simplest rate equation was employed, biofilm models are still relatively

complex because the microbial conversion of substrate is coupled with the diffusive transport of soluble substrates inside the biofilm. Thus, the substrate concentration varies not only with time but also with location within the biofilm. Biomass balances in bulk solution and inside the biofilm result in coupled simultaneous partial differential equations that are mathematically complex even for steady state single-substrate single-microorganism biofilm system. The difficulty is further augmented in dynamic systems. Early biofilm modeling approaches simplified the process by assuming that the process is at steady state, the biofilm thickness is constant and the microbial distribution within the biofilm is predetermined [31-35]. Microbial species distribution both in time and space was considered in the models of Kissel *et al.* [36] and Wanner and Gujer [37]. These models made the prediction of microbial species distribution as a function of substrate flux possible. The model of Rittmann and Manem [38] predicts species distribution within the steady state multispecies biofilm. The heterogeneous structure of the biofilm was considered in the researches of Lewandowski *et al.* [39], Zhang and Bishop [40], and Bishop [41]. Quantitative analysis of biofilm heterogeneity was performed in the mixed culture biofilm model of Wanner and Reichert [42]. Lewandowski *et al.* [43] defined textural entropy, areal porosity, fractal dimension and maximum diffusion distance as the quantitative parameters for describing the structure of a biofilm. With the current trend in biofilm modeling, the model continuously becomes complex as attempts are made to make it more realistic. However, as pointed by Holmberg and Ranta [44] modeling must be a compromise between making the model extensive enough to be realistic and reducing the number of parameters to a level at which they can be estimated from available data.

Methods to obtain the solution to these models were developed. The effectiveness factor method of Fink *et al.* [45] was applied in biofilm model. The effectiveness factor corrects for the effect of mass transport when the reaction rate at any point within the bioreactor is defined by the intrinsic reaction rate expressed in terms of the bulk concentration. Numerical values of this factor can be obtained from the plot of overall effectiveness factor against modified Thiele modulus at various Biot numbers [46]. Saez and Rittmann [47] developed the simplified pseudoanalytical solution for steady state biofilm. This solution is based on the analysis of the numerical results of differential equations. It eliminates the need for repetitiously solving a set of nonlinear differential equations. Using pseudoanalytical approach to solve for the substrate flux associated with various bulk substrate concentrations, Heath *et al.* [48] introduced the normalized loading curve approach to biofilm reactor analysis and design. In process identification, Rittmann *et al.* [49] developed an *in situ* kinetic parameter determination using curve matching technique.

Another approach to solve the problem was using direct numerical integration of the simultaneous partial differential equations. Software packages that can perform numerical integration are currently available (*e.g.*, MATLAB) [50]. Simulation programs specifically for water systems had been developed such as AQUASIM [51]. Horn and Hempel used direct numerical integration to simulate the long-term experiment on autotrophic biofilm growth and auto-/heterotrophic biofilm system. With fast computers, direct simulation is

easy if the kinetic parameters and other system constants were all known [52, 53]. However, for process identification purposes, finding the kinetic parameters and system constants for a system of nonlinear partial differential equations from sets of experimental data is still a difficult and tedious task. Simplifying assumptions have to be employed so that process identification is possible.

## 1.2.5 Step change analysis

The response of the system to step change in one of the input variables has been widely used to study the transient behavior of the system as well as to determine the constant parameters of the model that describes the system. The transient solution of the set of differential equation governing the system provides dynamic information such as the order of the step response, time constant, damping factor and process gains, which are essential to the design of control devices of the bioreactor. The steady-state solution is also included in the unsteady-state solution as its limit as time approaches infinity [54]. Step change experiment is an effective way for process identification, that is the determination of the form of the model equations as well as the constant parameters in those equations. Tang et al. [55] in their study of the dynamics of draft tube three-phase fluidized bed bioreactor stressed out the importance of the study of dynamic behavior of the fluidized bed bioreactor because the bioreactor operation is always in the transient condition during start-up and shutdown. Aside from that, it is also constantly exposed to disturbances such as diurnal variations and shock loading in inlet concentration and flow rates. Using phenol as the substrate, Tang's model considered external mass transfer resistance, simultaneous diffusion and reaction. As already discussed in [56], these models are theoretically thorough but also mathematically so complex that accurate process identifiably seems to be impossible. Modeling attempts of the transient state operation of the solid–liquid fluidized bed biofilm reactors were done by several researchers [57–59]. Worden and Donaldson [60] studied the dynamics of a fixed film fluidized bed bioreactor. Steady-state characteristics of the three-phase fluidized bed reactors have been investigated by Hirata et al. [61] and the basic design method for plug-flow type fluidized bed bioreactor has been proposed by Hirata and Noguchi [62]. Nevertheless, the standardized kinetic model that could be applied to biofilm processes in a practical use has not yet been established. In addition, it was reported that biofilm also has an active reservoir site for dissolved organic compounds via ion exchange and hydrophobic adsorption by extracellular polymer substances (EPSs) that are composed of polysaccharides, proteins, nucleic acids, lipids and other biological macromolecules [63, 64]. Therefore, it is necessary to illuminate the oxygen concentration profile inside biofilm.

## 1.2.6 Membrane science

The modification of the surface by the grafting method improved the adhesivity of some bacteria to the polyethylene membrane [65]. To facilitate bacterial adhesion to the

membrane surface, radiation-induced graft polymerization (RIGP) was used in our previous work [66]. This technique enables the modification of various polymeric backbones to open interfaces, which support the "grafting" of functional groups. Our groups successfully promoted bacterial adhesion via electrostatic interaction [69]. This method is expected to make the biofilm form swiftly and firmly, resulting in effective oxygen supply to specific bacteria.

### 1.2.7 Membrane aeration biofilm reactor

In biofilm processes, an oxygen concentration gradient is created acrossing the aggregated microorganism, so that both aerobic and anaerobic conditions can be established inside a single reactor [67]. A simultaneous nitrification and denitrification system in a single reactor, using a membrane-aerated biofilm reactor (MABR), was proposed. The MABR system can fix a biofilm onto the outside surface of a membrane, and can directly supply oxygen from the inner side to the biofilm. Casey *et al.* described the mechanism of this simultaneous nitrification and denitrification biofilm system [68]. This method contained the advantages: 1) accumulation of bacteria was enhanced by chemical modification of a membrane surface, 2) the amount of oxygen supplied was controlled by the intra-membrane pressure. We have succeeded in promoting the adhesivity and biofilm formation of nitrifying bacteria onto membranes modified with a grafted polymer chain [69]. In the newest research using the MABR, removal of xylene [70], phenol [71], chlorophenol [72] and acetate [73], treatment of hypersaline wastewater [74], nitrification [75], and simultaneous organic carbon removal and nitrification [76] were carried out. The simultaneous nitrification and denitrification using the MABR was suggested [77]. However, it is not directly verified whether the simultaneous nitrification and denitrification occurred inside or outside the biofilm in the MABR.

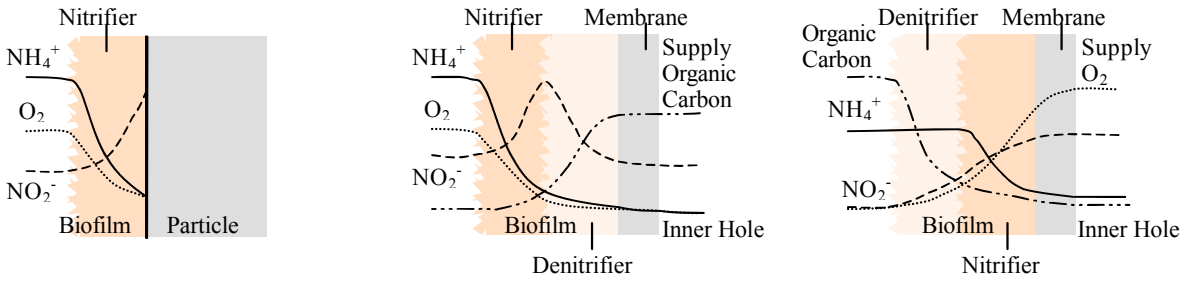


**(a)Conventional Biofilm Structure** **(b)New Biofilm Structure Type A** **(c)New Biofilm Structure Type B**

**Fig.1.1 Biofilm Structure in Membrane Bioreactor**

## 1.3 OBJECTIVE OF THIS STUDY

The main purpose of this study is to clarify the distribution of substrate concentration inside biofilm, especially the distribution of oxygen concentration in the wastewater treatment processes and applied above information to the improvement of treatment activity and development of new processes.

# Chapter II

**DEVELOPMENT OF MICROELECTORDE**

**Measuring Distributions of Substrate Concentration inside Biofilm by Ion-selective Microelectrodes and an Oxygen Selective Microelectrode**

## 2.1 INTRODUCTION

In this chapter, oxygen, ammonium-ion, and nitrate-ion concentrations and pH in the biofilms of several kinds was measured using original fabricated microelectrodes. Two different treatment systems run for organic carbon wastewater and inorganic carbon wastewater. This microelectrode method is most important in this study. Furthermore, microbial distribution inside biofilm was determined by fluorescence in situ hybridization (FISH) method.

## 2.2 BIOFILM FROM ORGANIC TREATMENT SYSTEM

### 2.2.1 MATERIALS AND METHODS

#### 2.2.1.1 Reactor system

A complete-mixing three-phase fluidized bed reactor was used for continuous nutrient oxidation. The effective volume of the reactor was 3 L. The reactors were operated with a hydraulic retention time (HRT) of 5 h. A cement ball (CB) fabricated from coal ash was used as the carrier particle on which biofilms were formed. The particle had an average diameter of 0.23 mm and a density of 1.92 g/cm$^3$. The temperatures of the feed tank and reactor were maintained at 5 and 20 ºC, respectively, using a thermostat. Sufficient air was supplied using an air pump to maintain a bulk oxygen concentration of about 3-4 g/m$^3$. Artificial wastewater composed of the chemicals shown in Table 2.1 was used.

The quality of this wastewater corresponds to a biochemical oxygen demand ($BOD_5$) of 600 g/m$^3$, a total organic carbon (TOC) content of 400 g/m$^3$, a total nitrogen (T-N) content of 200 g/m$^3$ and an ammonium-nitrogen ($NH_4^+$-N) content of 100 g/m$^3$. For water quality analysis, TOC content was measured using a TOC meter (Shimadzu, TOC-5000),

ammonium-ion content was measured using an ion chromatograph (DIONEX, DX120), nitrite and nitrate contents were measured using a high-performance liquid chromatograph (HPLC) equipped with an anion column (Tosoh, IC-Anion-PW) and an ultraviolet detector (Tosoh, UV-8011), and dissolved oxygen content was measured using an oxygen-selective electrode potentiometer (TOA, DO-11P). T-N was analyzed in accordance with the Standard Methods for the Examination of Water and Wastewater [20]. All samples were filtered through a glass filter (Whatman, GF/C) before analysis.

**Table 2.1 Composition of artificial wastewater [g/L]**

| | |
|---|---|
| Dextrin | 0.122 |
| Meat extract | 0.298 |
| Yeast extract | 0.262 |
| Bacto peptone | 0.262 |
| Sodium chloride (NaCl) | 0.026 |
| Magnesium sulfate ($MgSO_4 \cdot 7H_2O$) | 0.034 |
| Potassium dihydrogen phosphate ($KH_2PO_4$) | 0.074 |
| Potassium chloride (KCl) | 0.054 |
| Ammonium chloride ($NH_4Cl$) | 0.327 |
| Sodium bicarbonate ($NaHCO_3$) | 0.766 |

#### 2.2.1.2 Biofilms

Biofilms were grown in a continuously operated reactor. After one month of growth, biofilms of 200-300 $\mu$m thickness were obtained. Furthermore, biofilm thickness gradually increased, exceeding 1 mm after 2 years of operation. The biofilms had a fast growth rate because of the high loading rate and high amount of biodegradable substrate. Five experimental runs started at different times were simultaneously conducted. From these runs, biofilms of different thicknesses were obtained. Biofilm thickness was calculated from the image obtained by optical microscopy (BH-2, Olympus Co.) [3].

The biofilms of different thicknesses were randomly sampled. The number, equivalent diameter, wet volume and dry weight were measured for many biofilms. The overall biofilm dry density was calculated using each biofilm thickness.

Recently, many researchers have reported that biofilms are heterogeneous, and have conducted mathematical modeling of heterogeneous biofilms [21, 22]. Moreover, the density and porosity of biofilms change in the depth direction [23]. Therefore, two types of biofilm, of 120 and 1200 $\mu$m thicknesses were sampled. The biofilm samples were immediately fixed in freshly prepared 4% paraformaldehyde solution for 20 h. A 20-$\mu$m-thick biofilm section was prepared using a cryostat (Leica, CM-3050) at -20 ºC. Each slice was observed using a reflection light microscope with high resolution (Keyence,

VH-7000). The internal physical structure of the biofilms was visualized.

#### 2.2.1.3 Dissolved Oxygen Microelectrode

Oxygen concentration was measured with a Clark-type microelectrode. The microelectrode was fabricated in our laboratory as described by Revsbech [24]. The tip of the microelectrode was 5 $\mu$m in diameter and its time response of 90% ($t_{90}$) was about 10 s. Linear calibration was carried out in an air-saturated medium and a medium containing 300 mM $NaSO_3$ and a small amount of $CoCl_2 \cdot 6H_2O$ with nearly zero oxygen concentration.

The position of the biofilm surface was determined visually under a dissection microscope. The biofilms were fixed on a glass plate filled with a solution obtained from the reactor. All measurements were performed at 20 °C within several minutes. Then, the oxygen microelectrode was inserted into the biofilms in 10 $\mu$m steps using a micromanipulator (Narishige, MMO-203) to measure the spatial distribution of oxygen in the biofilms.

## 2.2.2 RESULTS AND DISCUSSION

#### 2.2.2.1 Oxygen penetration depth

Using an oxygen microelectrode, the oxygen distribution in the biofilms was measured while maintaining the bulk oxygen concentration at about 3 $g/m^3$. Examples of the experimental profile and the curves fitted for the exponential equation in the case of biofilms with 425 and 980 $\mu$m thicknesses are shown in Figure 2.3. As a result, we found that oxygen was gradually eliminated by bacteria in the biofilm and the liquid film formed in the bulk near the biofilm surface by the reaction. Oxygen penetration depth was determined from the obtainable oxygen distribution in the biofilms. Oxygen penetration ratio was calculated by dividing the oxygen penetration depth by the biofilm thickness.

The results of the oxygen penetration depth and ratio are shown in Figure 3.7. Oxygen diffused completely into the bottom of the biofilm of less than 300 $\mu$m thickness and oxygen penetration depth increased with increasing biofilm thickness. Oxygen penetration ratio gradually decreased with increasing biofilm thickness. Therefore, there is a large anaerobic zone at the bottom of the thick biofilm, indicating the possibility of microbial denitrification. Pochana et al. [29] considered the denitrification activity in the anaerobic zone in a floc and simulated the distribution of oxygen in the floc. Dalsgaard et al. [30] reported that denitrification activity in the anaerobic zone in a biofilm is computed from the mass balance equation using microelectrode analysis and that the denitrification zone is specified. However, the anaerobic zone is not necessary for oxidation processes such as carbon oxidization and nitrification. The thin biofilm without an anaerobic zone is effective for oxidation processes from the standpoint of obtaining a larger aerobic zone throughout the entire biofilm.

**Table 2.2 Water quality in the runs using thin or thick biofilms**

| | Thin biofilm ($d$ = 120 $\mu$m) | Thick biofilm ($d$ = 1200 $\mu$m) |
|---|---|---|
| TOC, g/m$^3$ | 15.6 | 42.1 |
| T-N, g/m$^3$ | 156.2 | 73.4 |
| $NH_4^+$-N, g/m$^3$ | 44.0 | 34.4 |
| $NO_2^-$-N, g/m$^3$ | 97.2 | 14.3 |
| $NO_3^-$-N, g/m$^3$ | 6.4 | 35.3 |
| DO, g/m$^3$ | 3.7 | 3.5 |
| Biofilm packing ratio, % | 20 | 20 |
| Ratio of carbon removal, % | 95.5 | 88.0 |
| Ratio of nitrification, % | 67.4 | 76.4 |
| Ratio of nitrogen removal, % | 3.2 | 54.5 |

#### 2.2.2.2 Water quality

The water treatment experiment was continuously carried out using the two reactors with the thin (representative biofilm thickness: 120 $\mu$m) and thick (representative biofilm thickness: 1200 $\mu$m) biofilms. Table 2.2 summarizes the water quality data of the effluent of each reactor in the steady state. The removal efficiency of TOC was high in the reactor with the thin biofilm because oxygen completely diffused into the bottom of the biofilm, and thus all biomass inside the biofilms contributed to the oxidation of organic compounds. In contrast, the removal efficiency of TOC in the reactor with the thick biofilm was lower than that with the thin biofilm, probably because the population of oxidizing bacteria was relatively small due to the existence of the anaerobic zone inside the biofilm, as determined based on the FISH results.

## 2.2.3 CONCLUSIONS

The oxygen distribution in biofilms was measured using an oxygen microelectrode that we fabricated. Oxygen penetration depth and ratio were computed based on the oxygen distribution. When the oxygen concentration in the bulk was 3 g/m$^3$, oxygen penetrated completely into the biofilms of less than 300 $\mu$m thicknesses. Oxygen penetration ratio gradually decreased with increasing biofilm thickness.

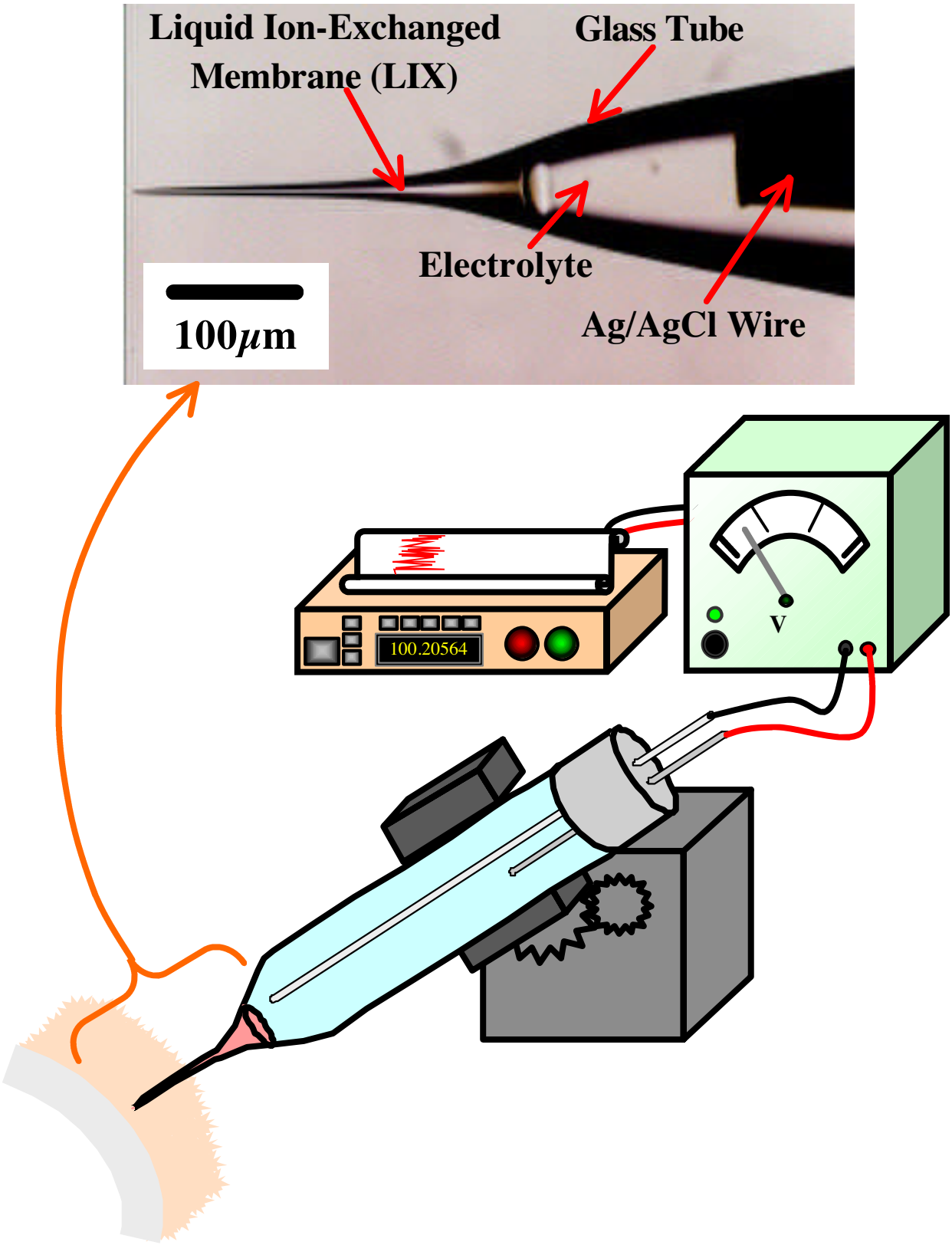


**Figure 2.1 Liquid ion-selective exchanged microelectrode and concept image of microelectrode system**

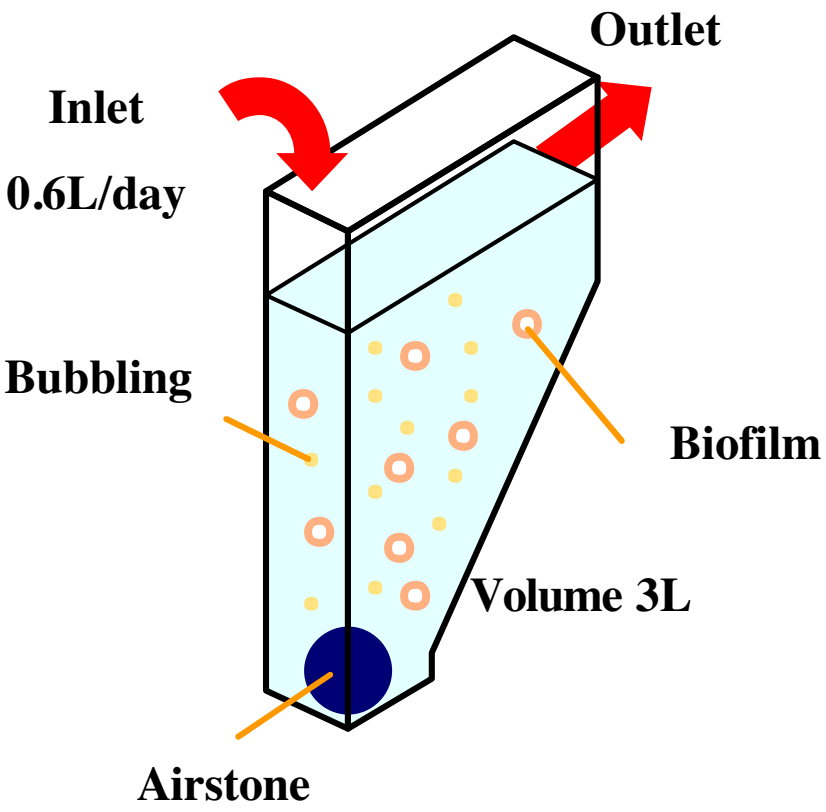


(a) Reactor system

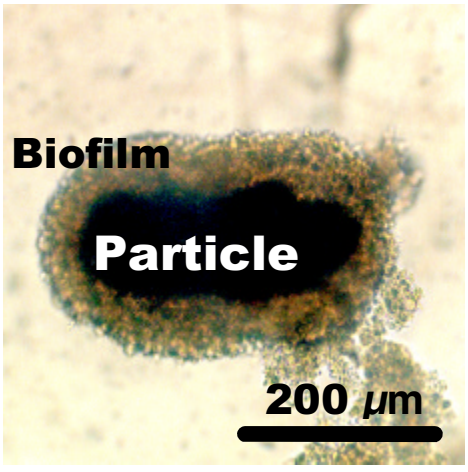


(b) Biofilm sample

**Figure 2.2 Fluidized-bed biofilm reactor system and image of biofilm slice sample**

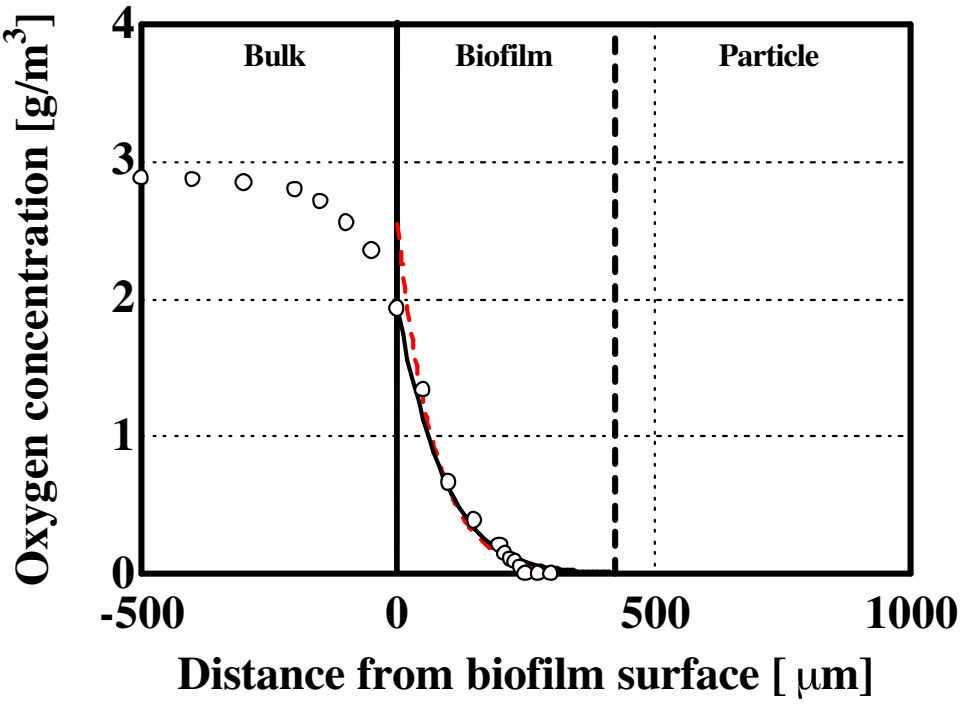


(a)

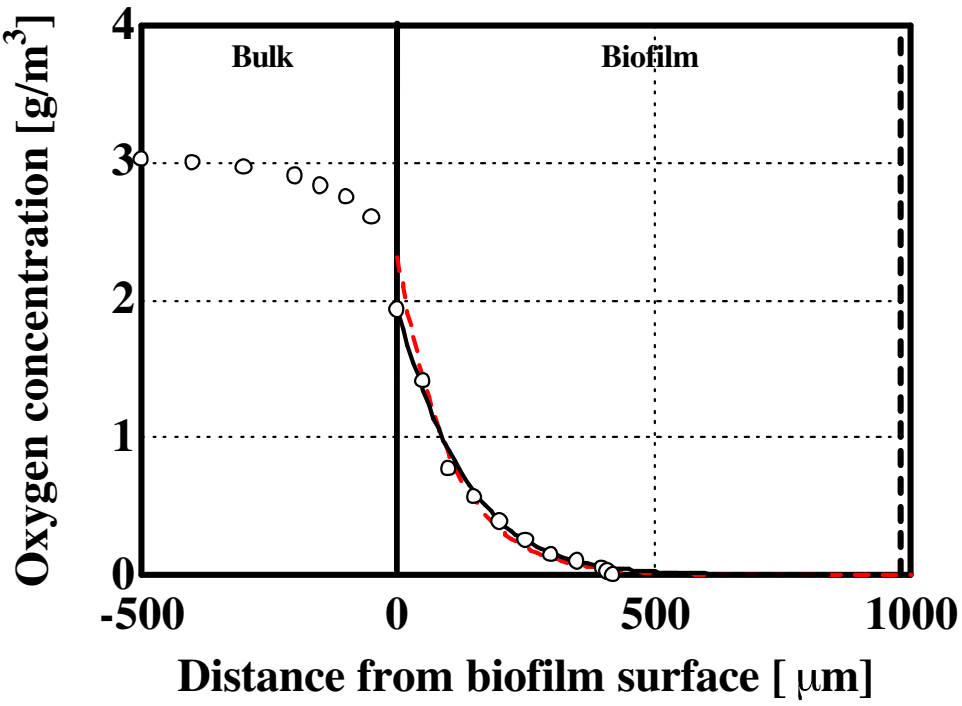


(b)

**Figure 2.3 Distribution of oxygen concentration inside biofilms of (a) 425 $\mu$m and (b) 980 $\mu$m thicknesses (open circles: experimental data from microelectrode analysis; broken line: fitted curve for exponential equation; continuous line: simulated curve)**

# 2.3 BIOFILM FROM INORGANIC TREATMENT

## 2.3.1 MATERIALS AND METHODS

### 2.3.1.1 Reactor System

The above-described substrate (600 g-N/$m^3$) was continuously fed at 1.0 L/day to a fluidized bed bioreactor with an effective volume of 2 L. The unmodified and modified membranes were used as supporting materials on which biofilms were immobilized. The temperature was maintained at 30℃. Air was supplied to the reactor at a suitable rate to fully disperse the biofilms and to provide excess dissolved oxygen. The pH of the solution in the reactor was adjusted to 7.5-8.0 by the addition of 1 *M* NaOH 1-3 times a day.

**Table 2.3 Composition of artificial wastewater (g/L)**

| | |
|---|---|
| $(NH_4)_2SO4$ | 2.83 |
| $KH_2PO_4$ | 0.5 |
| $K_2HPO_4$ | 1.0 |
| $FeSO_4$ | 0.05 |
| $MgSO_4 \cdot 7H_2O$ | 0.3 |
| $CaCl_2 \cdot H_2O$ | 0.002 |
| $MnCl_2 \cdot 4H_2O$ | 0.2 |
| $Na_2MoO_4 \cdot 2H_2O$ | 0.1 |

All culture samples were filtered through a 0.2-$\mu$m-pore-size membrane filter (Isopore®, Millipore Co.) prior to water quality measurement. The amount of organic pollutants was evaluated as total organic carbon (TOC) with an automatic TOC analyzer (TOC-500, Shimadzu Co.). Ammonium-nitrogen ($NH_4^+$-N) was determined using an ammonia-selective electrode (F-203, Horiba Co., Japan). Nitrite-nitrogen ($NO_2^-$-N) and nitrate-nitrogen ($NO_3^-$-N) were determined using an ion-chromatograph system (IC-Anion-PW, UV-8011, Tosoh Co.). Biofilm thickness was calculated from the image obtained by optical microscopy (BH-2, Olympus Co.). Bacterial adhesion to membranes was confirmed from SEM (S-2500, Hitachi Co.) images.

### 2.3.1.2 Biofilms

Biofilms were grown in a continuously operated reactor. The thickness of biofilm on the grafted membrane was approximately 20 $\mu$m at day 88 and approximately 100 $\mu$m at day 150. In contrast, no biofilm was formed on the unmodified membrane. From these runs, biofilms of different thicknesses were obtained. Biofilm thickness was calculated from the image obtained by optical microscopy (BH-2, Olympus Co.) .

The biofilms of different thicknesses were randomly sampled. The number, equivalent diameter, wet volume and dry weight were measured for many biofilms. The overall biofilm

dry density was calculated using each biofilm thickness.

Recently, many researchers have reported that biofilms are heterogeneous, and have conducted mathematical modeling of heterogeneous biofilms. Moreover, the density and porosity of biofilms change in the depth direction. Therefore, two types of biofilm, of 120 and 1200 $\mu$m thicknesses were sampled. The biofilm samples were immediately fixed in freshly prepared 4% paraformaldehyde solution for 20 h. A 20-$\mu$m-thick biofilm section was prepared using a cryostat (Leica, CM-3050) at -20 ºC. Each slice was observed using a reflection light microscope with high resolution (Keyence, VH-7000). The internal physical structure of the biofilms was visualized.

#### 2.3.1.3 Liquid Ion-Selective Membrane (LIX) Microelectrodes

Liquid ion-exchange membrane (LIX) microelectrodes for pH and $NH_4^+$ were prepared as described by de Beer *et al*. [7]. Using a micropipettpuller (MPT-1, Shimadzu Co.), 1-mm-diameter soda lime glass tubes (100 $\mu$L Micropipetts, Drummond Co.) were drawn into microcapillaries. The tip diameter was about 5 $\mu$m for all LIX microelectrodes and the tips of the electrodes were silanized with 20% (vol/vol) solution of trimethylchlorosilane in carbon tetrachloride to obtain a hydrophobic surface for optimal adhesion of the LIX membranes. After the tips of the microelectrodes were filled with the silanized-solution, the electrodes were baked for at least 1 h at 130℃ to remove traces of water. The liquid membrane used was 10% (wt/wt) tridodecylamine and 1% (wt/wt) sodium tetraphenylborate in 2-nitrophenyloctyl ether for pH microelectrode and 10% (wt/wt) nonactine and 1% (wt/wt) sodium tetraphenylborate in 2-nitrophenyloctyl ether for $NH_4^+$ microelectrode. The filling electrolytes used were 0.04 *M* $KH_2PO_4$, 0.023 *M* NaOH and 0.015 *M* NaCl for pH microelectrode and 0.01 *M* $NH_4Cl$ for $NH_4^+$ microelectrode. Finally, Ag/AgCl wires were inserted into the capillaries and fixed using epoxy.

The pH microelectrode was calibrated in adjusting series of the substrate by 1 *M* NaOH or 1 *M* HCl. The $NH_4^+$ microelectrode was calibrated in dilution series of $NH_4^+$ in the medium for the experiment.

Nitrifying biofilms were taken out from the bioreactor at day 150 for microelectrode measurement. A biofilm was fixed on a glass plate that was filled with the solution obtained from the bioreactor. Then, pH and $NH_4^+$ microelectrodes were inserted into the biofilm at 10 $\mu$m steps using a micromanipulator (MMO-203, Narishige Co.) to measure the spatial distributions of pH and $NH_4^+$ inside the biofilms. Microprofiles were determined five times at different positions in the biofilms.

#### 2.3.1.4 Fluorescence in situ hybridization (FISH) method

The biofilm samples for FISH, which were taken out from the bioreactor at day 150,

were immediately fixed with 4% paraformaldehyde. A biofilm section of 20 $\mu$m thickness was prepared from the frozen biofilm sample embedded in OCT-compound using cryostat (CM3050, Leica Co.) at -20℃, and placed in a hybridization well on a gelatin-coated microscopic slide.

For hybridization of the biofilm sections on the slide, the standard hybridization protocol described by Amann was used [8]. Two 16S rRNA targeted oligonucleotide probes were used for *in situ* detection of ammonia-oxidizing and heterotrophic bacteria: (1) NSO190 (labeled with TRITC): specific for the region of the 16S rRNA of all ammonia-oxidizing bacteria of the $\beta$-subclass of proteobacteria [9]; (2) EUB338 (labeled with Cy5): a probe for targeting all bacteria [10]. After probing, slides were examined with a confocal laser-scanning microscope (TCS NT, Leica Co.).

## 2.3.2 RESULTS AND DISCUSSION

### 2.3.2.1 Substrate profile inside biofilms

The pH and $NH_4^+$-N profiles of nitrifying biofilms on the membranes were measured using microelectrodes. The results are shown in Figure 2.5 where the plots and error bars correspond to averages and standard deviations, respectively. Since $NH_4^+$-N sufficiently diffused into the deep zone of the biofilms, it was thought that the rate-limiting factors were not only substrate diffusivity but also biological reaction. Therefore, both larger specific biofilm surface area and thicker biofilm increase the nitrification rate. Because pH decreased gradually with increasing depth of in the biofilm, this implied that nitrification occurred at every part of the biofilm. In addition, the present biofilm was sufficiently thick to remove nutrients from wastewater, because in the case of biofilms thicker than the present one, nitrifying bacteria might lose their activity at low pH at the deep zone inside the biofilms.

### 2.3.2.2 Identification of bacteria inside the biofilm by FISH method

The FISH image of the biofilm that was taken out from the bioreactor at day 150 is shown in Figure 2.7. The biofilm was found consist of mostly autotrophic ammonia-oxidizing bacteria. This result is consistent with the substrate's composition, *i.e.*, large amount of ammonium-nitrogen without any organic carbon source. However, a microorganism that differed from ammonia-oxidizing bacteria, supposedly a nitrite-oxidizing bacterium, existed in small numbers in the biofilm.

### 2.3.2.3 Water quality

Membranes with nitrifying biofilm were introduced into a fluidized bed bioreactor where $NH_4^+$ as a nutrient was continuously fed. The results of water quality analysis are shown in

Figure 2.6. Biofilm thickness was observed every day by optical microscopy. Representative images of biofilms on the membranes are shown in Figure 5.3.

The thickness of biofilm on the grafted membrane was approximately 20 $\mu$m at day 88 and approximately 100 $\mu$m at day 150. In contrast, no biofilm was formed on the unmodified membrane. Therefore, a new supporting material suitable for biofilm formation was successfully developed by modification of the surface by the grafting method. Nitrification rate was very unstable until day 50 because of the small amount of attached and suspended nitrifying bacteria. However, after day 50, a thick biofilm was retained, and thus the $NH_4^+$-N removal rate reached as high as 0.3 kg-N/($m^3$·day) and became stable.

## 2.3.3 CONCLUSIONS

The profiles of pH and $NH_4^+$ inside the biofilms were successfully measured by using the originally fabricated the microelectrodes. $NH_4^+$-N removal rate per unit area of biofilm was calculated from the bulk concentration change and from the concentration profile inside the biofilm. As a result, this biofilm exhibited a markedly higher $NH_4^+$-N removal rate than other biofilms.

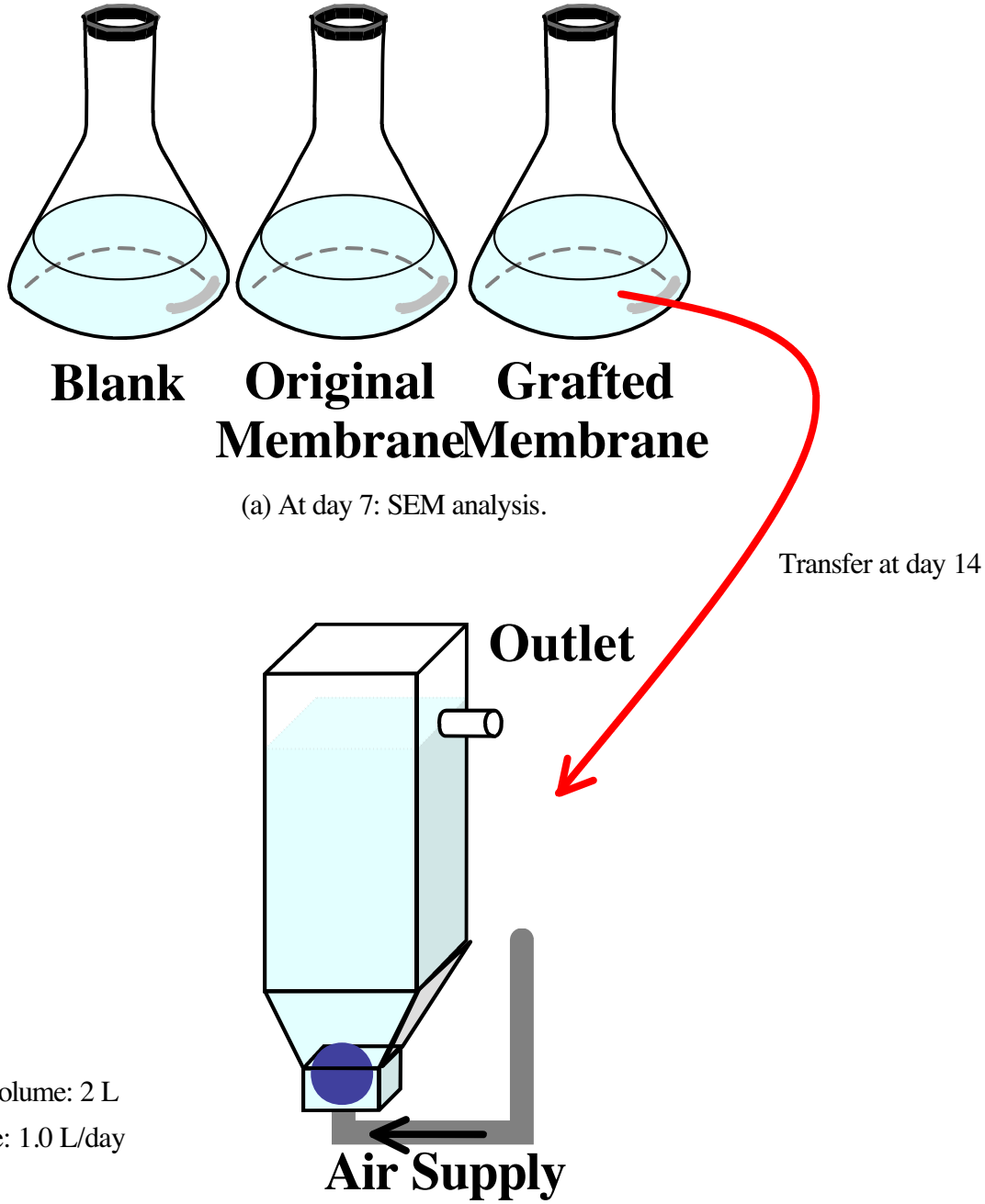


**Figure 2.4 Explain of batch and continuous experiment for bacterial attachment on original and grafted membranes**

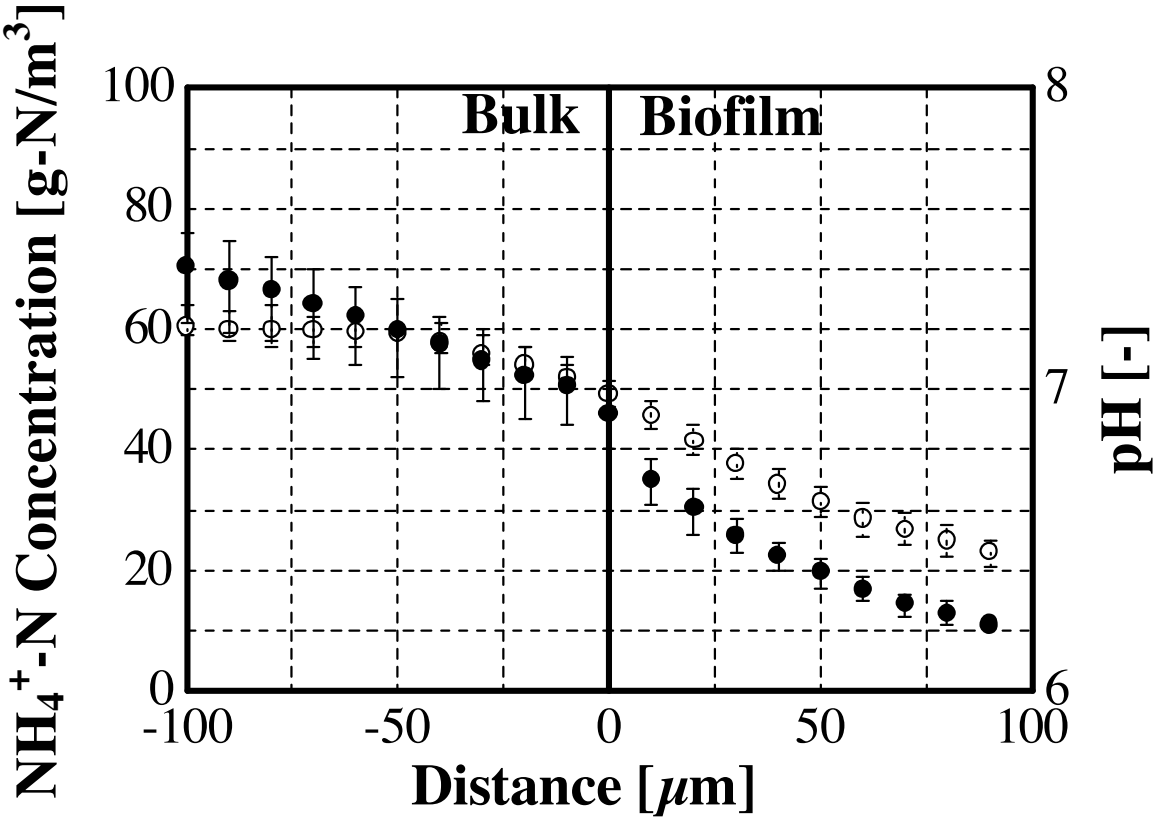


**Figure 2.5 The pH and $NH_4^+$-N profiles inside nitrifying biofilm on grafted membrane. $NH_4^+$-N (? ), pH (? )**

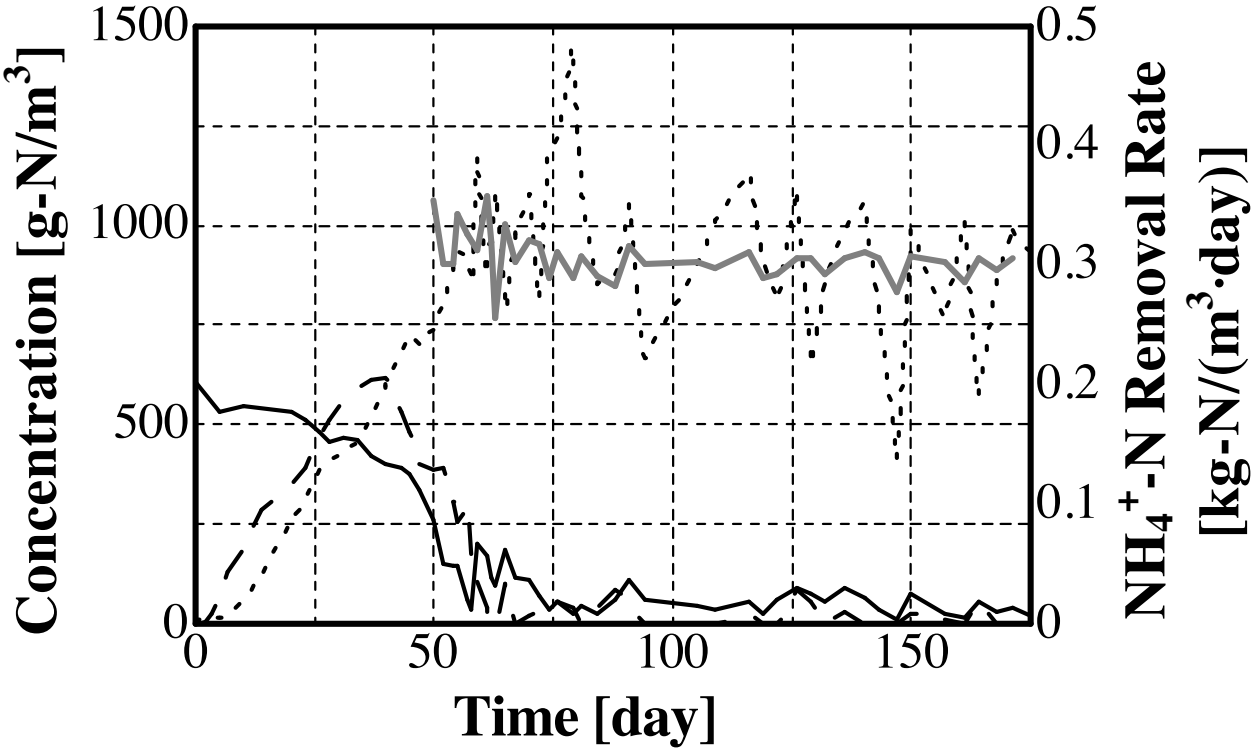


**Figure 2.6 Time course of nitrogen compounds concentration in fluidized bed bioreactor containing grafted membrane with nitrifying biofilm. $NH_4^+$-N ( ), $NO_2^-$-N ( ), $NO_3^-$-N ( ), $NH_4^+$-N Removal Rate ( )**

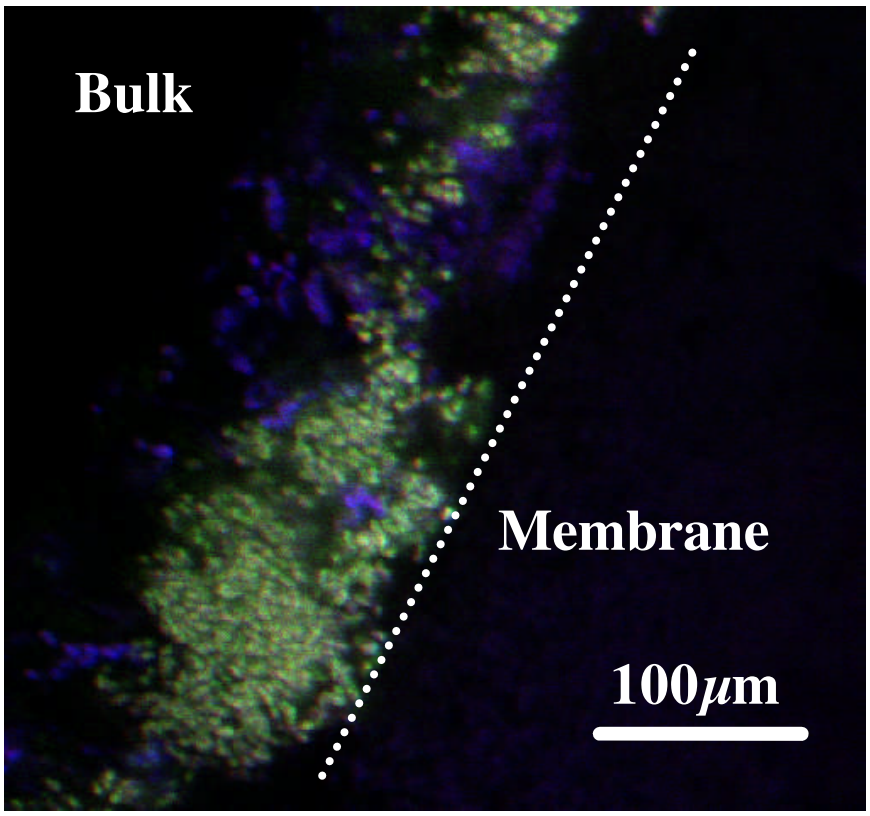


**Figure 2.7 FISH image inside biofilm at day 150 (×1000). Green yellow part shows ammonia oxidizing bacteria and purple part shows other bacteria**

# Chapter III

## SIMULATION INSIDE BIOFILM

**Simple Prediction of Oxygen Penetration Depth in Biofilms for Wastewater Treatment**

## 3.1 INTRODUCTION

In this chapter, oxygen concentration in the biofilms of several thicknesses was measured using an oxygen microelectrode, and was statistically simulated by the finite difference method at several biofilm thicknesses and bulk oxygen concentrations. The kinetic parameters and effective diffusion coefficients of oxygen in the biofilm, and the oxygen penetration depths were determined. As a result, the optimum thickness of the biofilms for oxidizing processes such as simultaneous organic carbon removal and nitrification in a fluidized bed reactor was determined.

## 3.2 MATERIALS AND METHODS

### 3.2.1 Simulation

The oxygen distribution in the biofilms was simulated with a Monod equation with regard to oxygen consumption through biological reaction. The parameters were determined in accordance with the method of Lewandowski [25]. The calculation method is as follows: The mass balance equation for oxygen in the biofilms is

$$\frac{dC}{dt} = D_e \frac{d^2C}{dx^2} - \frac{k \cdot X \cdot C}{K_m + C}, \qquad (1)$$

where $C$ is the oxygen concentration, $t$ the time, $D_e$ the effective diffusion coefficient of oxygen in the biofilms, $x$ the distance from the biofilm surface, $k$ the reaction rate constant, $K_m$ the Monod saturated constant, and $X$ the dry density of the biofilms. When the steady-state concentration profile of the inside of a biofilm is achieved, the consumption rate is equal to diffusion rate. Then, taking the inverse of each part in Equation (1) yields the function between the inverse of the second derivative and the inverse of oxygen concentration as

$$\left(\frac{d^2C}{dx^2}\right)^{-1} = \frac{D_e \cdot K_m}{k \cdot X} \cdot \frac{1}{C} + \frac{D_e}{k \cdot X} . \qquad (2)$$

The slope ($D_e \cdot K_m/k \cdot X$) divided by the intercept ($D_e/k \cdot X$) yields $K_m$. The second derivative is calculated using the exponential equation (Equation (3)) that fits to the experimental profile of oxygen distribution in the biofilms. The exponential equation was best fitted for the experimental data.

$$C = a_1 + a_2 \cdot \exp\left(-x / a_3\right) \qquad (3)$$

According to Frank-Kameneski [26], the mass balance equation at the steady state can be transformed to

$$\left(\frac{dC}{dx}\right)_f = \sqrt{2\frac{k \cdot X}{D_e}\left(C - K_m \cdot \ln\frac{K_m - C}{K_m}\right)}, \qquad (4)$$

where subscript *f* indicates film and $(dC/dx)_f$ is the gradient of oxygen concentration in the biofilm. Using the sets of parameters $k \cdot X/D_e$ and $K_m$ which were computed using Equation (2), the first derivative of oxygen concentration in the biofilm $(dC/dx)_f$ can be obtained.

Substrate molecules, before reaching the biofilm surface, must travel across the diffusion boundary layer. In idealized, perfectly stagnant water, the process would be entirely dependent on molecular diffusion. Consequently, the profile of oxygen concentration would be linear without convection. Therefore, the oxygen profile above the biofilm surface can be adequately described by the empirical exponential function

$$\frac{C - C_s}{C_b - C_s} = 1 - \exp\left\{-A \cdot \left(x - x_s\right)\right\}, \qquad (5)$$

where subscript *s* represents the interface between the biofilm and the bulk, subscript *b* represents the bulk and *A* is the experimental constant. The first derivative in the bulk $(dC/dx)_w$ is

$$\left(\frac{dC}{dx}\right)_w = A \cdot \left(C_b - C_s\right), \qquad (6)$$

where subscript *w* represents water and $(dC/dx)_w$ is the gradient of oxygen concentration in the bulk. By fitting Equation (5) to the experimental data obtained using the microelectrode, the slope of *A* is calculated and the first derivative in the bulk $(dC/dx)_w$ can be obtained.

Moreover, oxygen flux through the biofilm-bulk interface ($J_f$) and diffusion layer ($J_w$) are respectively defined as

$$J_f = D_f \cdot \left(\frac{dC}{dx}\right)_f , \qquad (7)$$

$$J_w = D_w \cdot \left(\frac{dC}{dx}\right)_w . \qquad (8)$$

Since oxygen flux at the biofilm-bulk interface is continuously preserved ($J_f = J_w$), the

internal diffusion coefficient in the biofilm is given as

$$D_e = D_f = D_w \cdot \frac{\left(\frac{dC}{dx}\right)_w}{\left(\frac{dC}{dx}\right)_f}. \qquad (9)$$

Using the diffusion coefficient of water at 21°C of $2.0\times10^{-9}$ $m^2/s$ [27], $(dC/dx)_f$ from Equation (4) and $(dC/dx)_w$ from Equation (6), the internal diffusion coefficient of the biofilm, $D_e$, can be computed. Moreover, $k$ was computed from the calculated values of $k\cdot X/D_e$ and $D_e$, and the experimental values of $X$. The average of all the values was represented.

The oxygen distribution is simulated using the calculated kinetics parameters, the dry density of the biofilm and diffusion coefficient of oxygen in the biofilm. The simulation was conducted using Equation (1) by the finite difference method ($dx = 10^{-5}$, $dt = 10^{-7}$, saturation $= 10^{-8}$, and max iterations $= 10^7$). The oxygen distribution inside the biofilm was simulated under the boundary conditions at the biofilm surface and at an infinite point from the biofilm surface. Oxygen penetration depth was determined from the simulation curve of the oxygen distribution in the biofilm.

## 3.3 RESULTS AND DISCUSSION

### 3.3.1 Density and porosity

Figure 3.1 shows the plots of dry density against biofilm thickness. Biofilm density decreased with increasing biofilm thickness. The dry density of the biofilm in the fluidized bed reactor was found to be 2-10 times higher than that ($X = 8700$ g/m$^3$) in the rotating disk reactor [28]. The empirical equation that shows the relation between dry density ($X$) and biofilm thickness ($d$) is

$$X = 2.5\times10^4+1.5\times10^5\cdot\exp(-d/175). \qquad (10)$$

Figure 3.2 shows the internal cross-sectional photographs of the biofilms of 120 and 1200 $\mu$m thicknesses, obtained using a light microscope. The thin biofilm had a dense homogenous structure. In contrast, the thick biofilm had a heterogeneous structure and large pores. Therefore, the thinner biofilm was expected to exhibit a lower substrate penetration depth because of the high-density structure which results in a small diffusion coefficient and high reaction rate.

### 3.3.2 Oxygen penetration depth

Using an oxygen microelectrode, the oxygen distribution in the biofilms was measured while maintaining the bulk oxygen concentration at about 3 g/m$^3$. Examples of the experimental profile and the curves fitted for the exponential equation in the case of biofilms with 425 and 980 $\mu$m thicknesses are shown in Figure 3.6. As a result, we found that oxygen was gradually eliminated by bacteria in the biofilm and the liquid film formed in the bulk near the biofilm surface by the reaction. Oxygen penetration depth was determined from the obtainable oxygen distribution in the biofilms. Oxygen penetration ratio was calculated by dividing the oxygen penetration depth by the biofilm thickness. The results of the oxygen penetration depth and ratio are shown in Figure 3.7. Oxygen diffused completely into the bottom of the biofilm of less than 300 $\mu$m thickness and oxygen penetration depth increased with increasing biofilm thickness. Oxygen penetration ratio gradually decreased with increasing biofilm thickness. Therefore, there is a large anaerobic zone at the bottom of the thick biofilm, indicating the possibility of microbial denitrification. Pochana et al. [29] considered the denitrification activity in the anaerobic zone in a floc and simulated the distribution of oxygen in the floc. Dalsgaard et al. [30] reported that denitrification activity in the anaerobic zone in a biofilm is computed from the mass balance equation using microelectrode analysis and that the denitrification zone is specified. However, the anaerobic zone is not necessary for oxidation processes such as carbon oxidization and nitrification. The thin biofilm without an anaerobic zone is effective for oxidation processes from the standpoint of obtaining a larger aerobic zone throughout the entire biofilm.

### 3.3.3 Determination of kinetic parameters and effective diffusion coefficient

Figure 3.3 shows the relationship between $(d^2C/dx^2)_f$ and $1/C$ for evaluating $K_m$ in the case of biofilms of 425 and 980 $\mu$m thicknesses. Then, $K_m$ could be calculated from the slope and intercept of the linear fit to the relationship between $(d^2C/dx^2)_f$ and $1/C$. The linear fit for all plots seemed to be impossible, as shown in Figure 4 (b). The linear line could be fitted only for low $1/C$ values, if low oxygen concentrations (below 0.2 g/m$^3$) are neglected. This concept is reasonable because only high oxygen concentrations affect oxidation rate. Then, the slope, $k \cdot X/D_e \cdot K_m$, and the intercept, $k \cdot X/D_e$, were obtained from the linear fitted curves within the range of the low $1/C$ values. The average $K_m$ calculated from the slope and intercept was 1.5 g/m$^3$.

The flux at the biofilm surface was calculated using Equation (4). Then, the flux at the diffusion boundary layer was calculated using Equation (5) with the empirical coefficient of $A$. Figure 3.4 shows an example of the plot for the evaluation of $A$. Since the flux continuity must be preserved at the biofilm-water interface ($J_f = J_w$), the effective diffusion coefficients were calculated for the distribution of oxygen in each biofilm. Figure 3.5 shows the calculated effective diffusion coefficients plotted against biofilm thickness. The calculated

diffusivity was 40 – 90% which is close to those reported by Stewart et al. [85]. The density-diffusivity correlation was in good agreement with the correlation proposed by Fan et al. [86]. From the result, the empirical equation showing the relationship between $D_e$ and $d$ was obtained.

$$D_e = (3.5^{-19} + 1.5^{-21} \cdot d)^{0.5} \qquad (11)$$

Moreover, $k$ was computed from $k \cdot X/D_e$ (calculated from Figure 3.1), $D_e$ and $X$ (determined from respective empirical equations). The representative $k$ was $7.5 \times 10^{-6}$ 1/s.

### 3.3.4 Simulation of oxygen distribution in biofilms

The boundary condition is given by the following equation as the data for oxygen concentration below 0.2 g/m$^3$ were adopted.

$$\begin{cases} x = x_s; \quad c = c_s \\ x = \infty; \quad c = 0.2 \end{cases} \qquad (12)$$

Figure 3.6 shows the plots of experimental data obtained using the microelectrode and the simulated curves of oxygen distribution in the biofilms of 425 and 980 $\mu$m thicknesses. The simulated curves successfully fit the experimental plots. Therefore, the oxygen distribution inside the biofilm can be simulated in the runs where sufficient concentrations of the substrates, that is, organic carbon and ammonia, were supplied, because in such cases, the consumption rates of each substrate and oxygen completely depend on local oxygen concentration. The good fittings indicate that the distribution of the substrate in the biofilm can be sufficiently simulated using a simple model.

Next, oxygen distribution in the biofilms was simulated at several biofilm thicknesses and oxygen concentrations in the bulk. Figure 3.7 shows the experimental plots of oxygen penetration ratio against biofilm thickness and their simulated curves. Therefore, the aerobic zone, which contributes to microbial oxidation, can be predicted at various biofilm thicknesses and oxygen concentrations in the bulk.

### 3.3.5 Water quality

The water treatment experiment was continuously carried out using the two reactors with the thin (representative biofilm thickness: 120 $\mu$m) and thick (representative biofilm thickness: 1200 $\mu$m) biofilms. Table 2.2 summarizes the water quality data of the effluent of each reactor in the steady state. The removal efficiency of TOC was high in the reactor with the thin biofilm because oxygen completely diffused into the bottom of the biofilm, and thus all biomass inside the biofilms contributed to the oxidation of organic compounds. In contrast, the removal efficiency of TOC in the reactor with the thick biofilm was lower than that with the thin biofilm, probably because the population of oxidizing bacteria was

relatively small due to the existence of the anaerobic zone inside the biofilm, as determined based on the FISH results (data not shown).

The thin biofilm exhibited a lower nitrification rate than the thick biofilm because there was no space in the bottom zone of the biofilm where the nitrifying bacteria could exist. An adequately thick biofilm is necessary for successful nitrification because of oxygen competition and the distribution of microbial heterotrophs and nitrifiers inside the biofilm. Thus, biofilms of 300 – 400 $\mu$m thickness may be appropriate for simultaneous carbon oxidation and nitrification in a fluidized bed reactor. Furthermore, the marked decrease in T-N content indicates that the thick biofilm had denitrification activity in the bottom zone in which oxygen concentration was nearly zero. In a fluidized bed reactor, we suggest that the biofilm thickness should be suitably controlled for objective treatment by aeration which is independent of operation conditions.

## 3.4 CONCLUSIONS

1. The kinetic parameters of a Monod reaction and the effective diffusion coefficient were calculated based on the oxygen distribution in the biofilms. The effective internal diffusion coefficient of the biofilms changed with biofilm density and biofilm thickness. The effective diffusivity ranged from 40% to 90%.

2. Using the results of biofilm dry density, kinetic parameters and effective diffusion coefficient, the oxygen distribution in the biofilms were successfully simulated using a one-dimensional model with a Monod reaction. It was demonstrated that oxygen penetration ratio, which markedly influences biological oxidation activity, can be determined using this simple simulation.

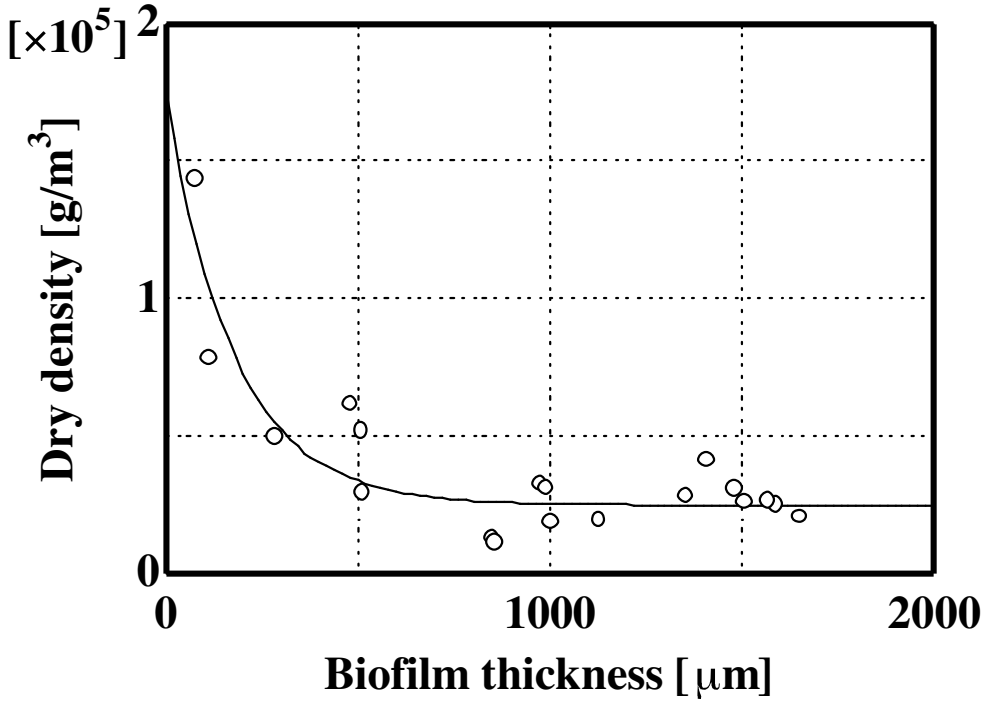


**Figure 3.1 Relationship between biofilm thickness and dry density for several biofilm samples (open circles: experimental data; continuous line: smooth curve ($X = 2.5\times10^4 + 1.5\times10^5 \cdot \exp(-d/175)$)**

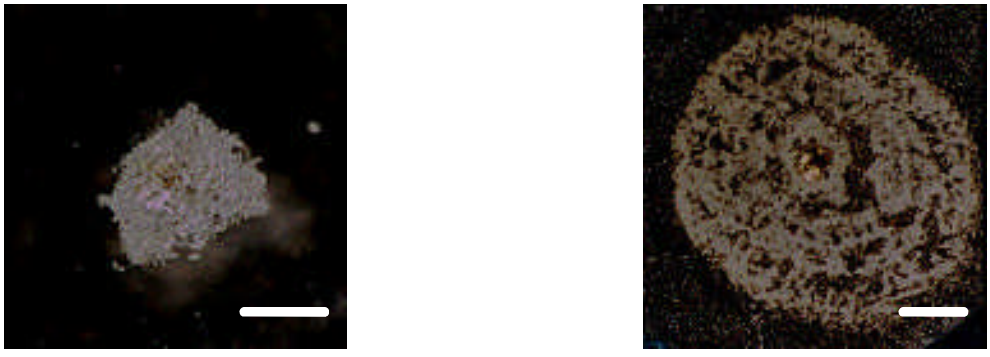

(a) (b)

**Figure 3.2 Internal physical structure of (a) thin biofilm (thickness: 120 $\mu$m; scale bar denotes 100 $\mu$m), and (b) thick biofilm (thickness: 1200 $\mu$m; scale bar denotes 500 $\mu$m) as observed by light microscopy**

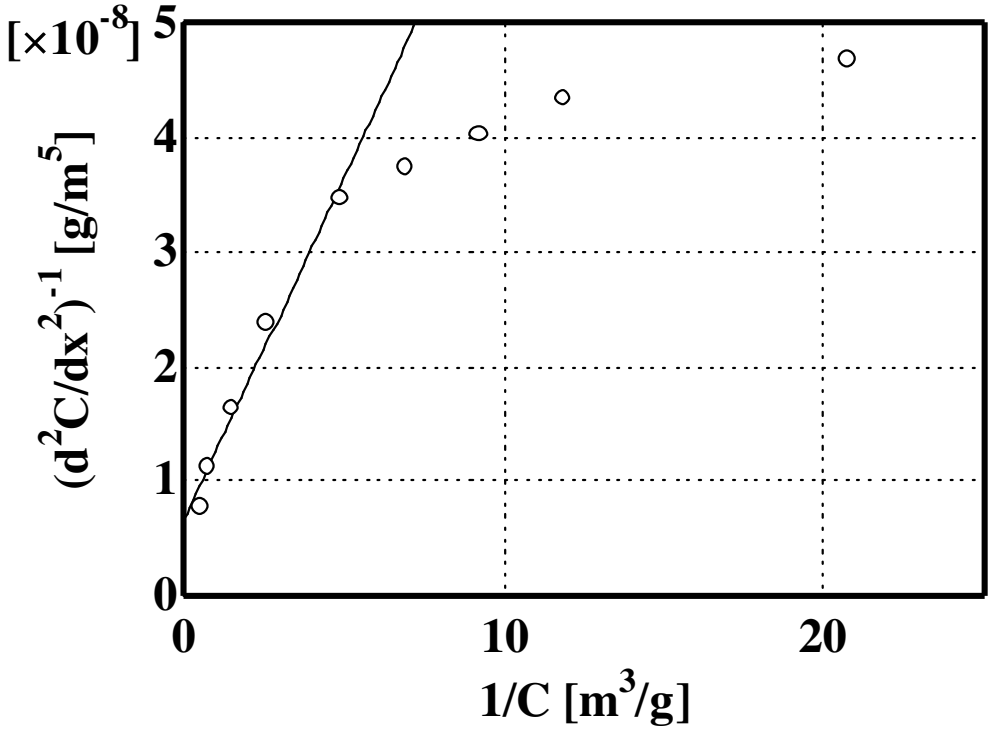


(a)

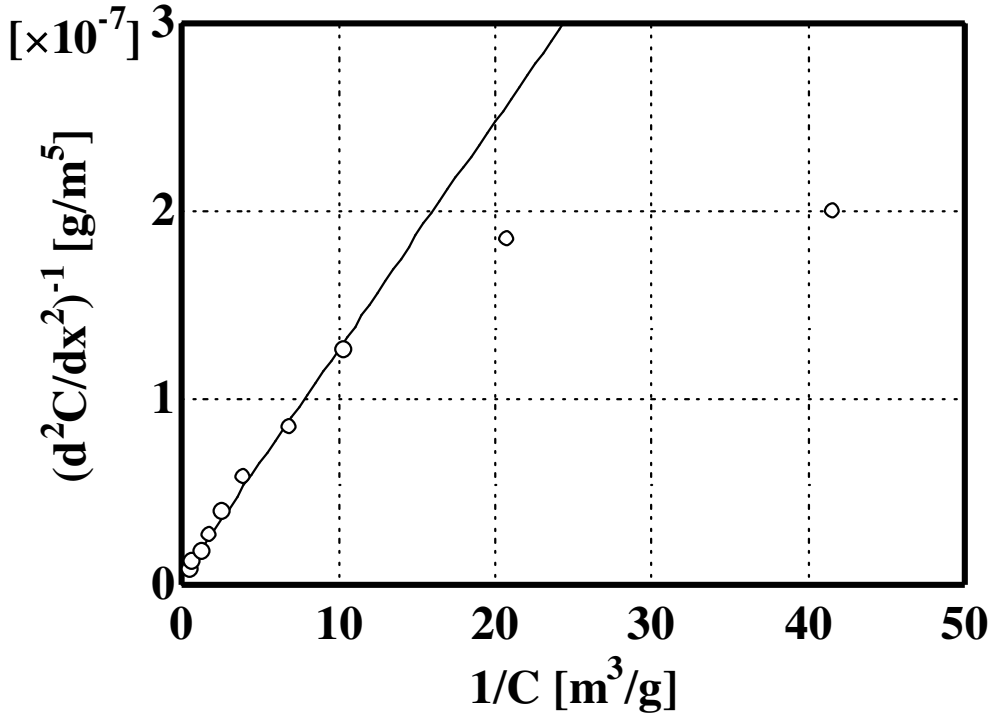


(b)

**Figure 3.3 Relationship between $(d^2C/dx^2)_f$ and $1/C$ for evaluating $K_m$ in the case of biofilm of (a) 425 $\mu$m and (b) 980 $\mu$m thicknesses (open circles: experimental data from microelectrode analysis; continuous line: empirically linear)**

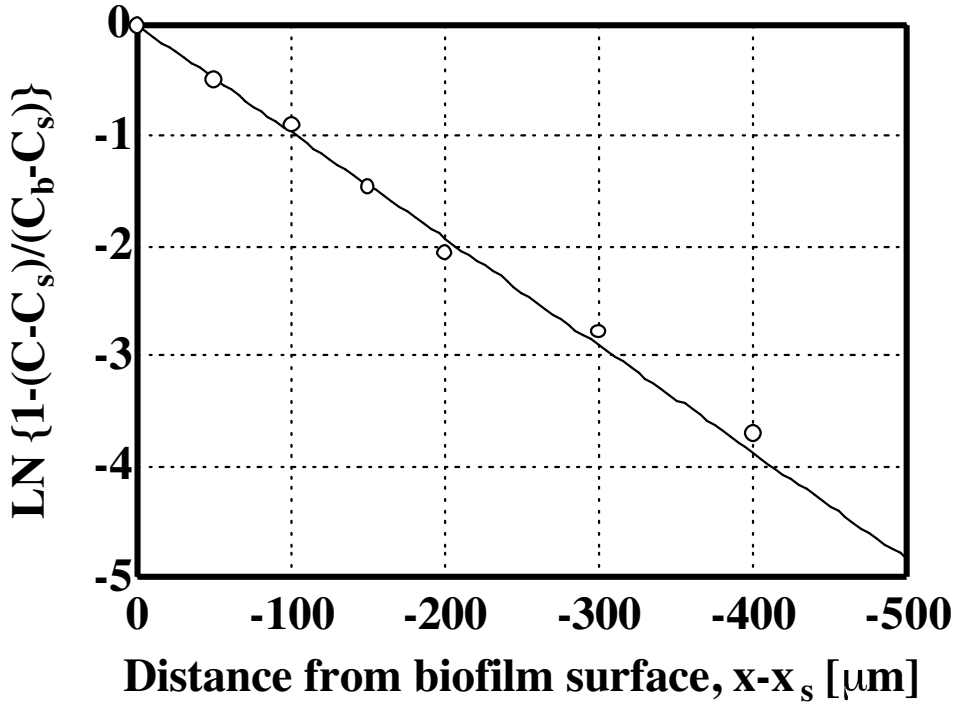


(a)

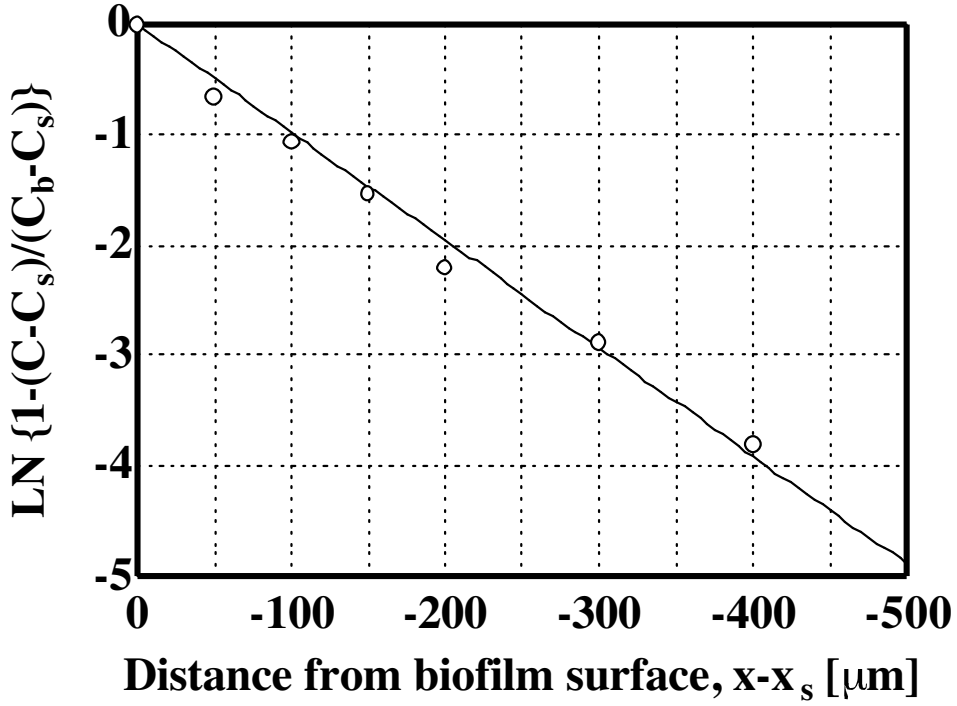


(b)

**Figure 3.4 Relationship between LN {1-($C$-$C_s$)/($C_b$-$C_s$)} and distance from biofilm surface, $x$-$x_s$, at a diffusion layer in the case of biofilms of (a) 425 $\mu$m and (b) 980 $\mu$m thicknesses (open circles: experimental data from microelectrode analysis; continuous line: empirically linear)**

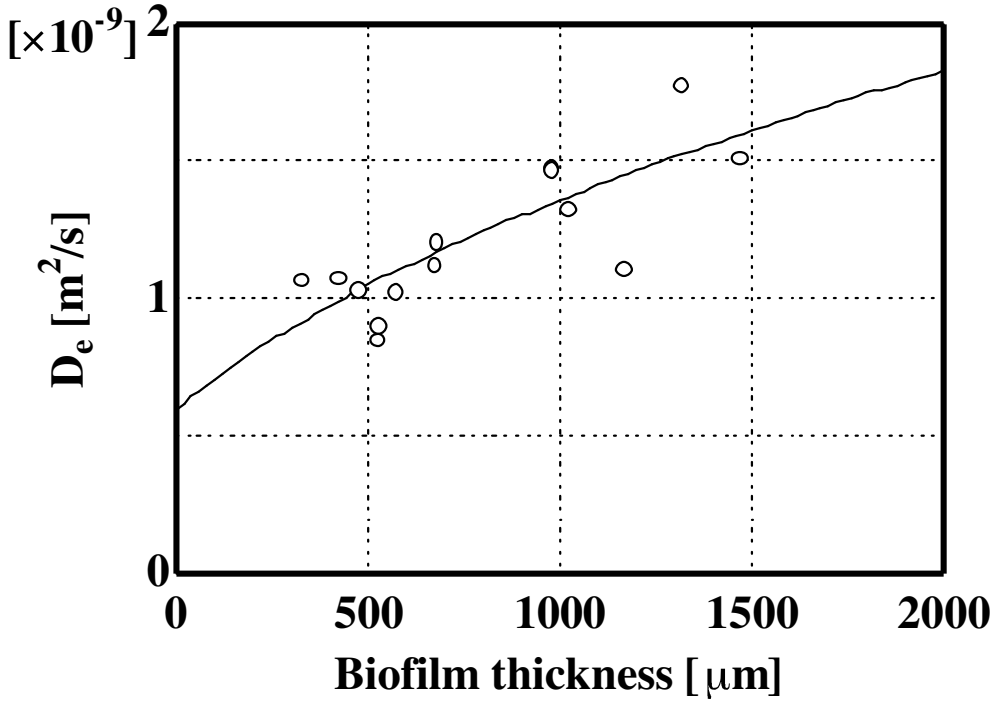


**Figure 3.5 Relationship between biofilm thickness and calculated effective diffusion coefficient for several biofilm samples. The empirical equation, $D_e = (3.5^{-19} + 1.5^{-21} \cdot d)^{0.5}$, is shown as a continuous line**

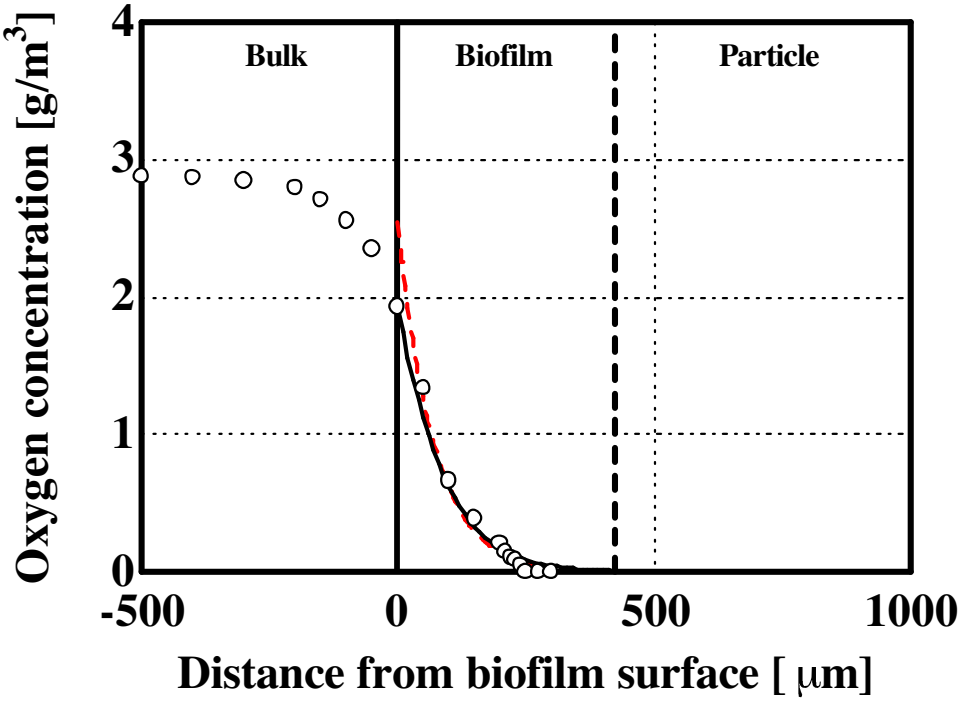


(a)

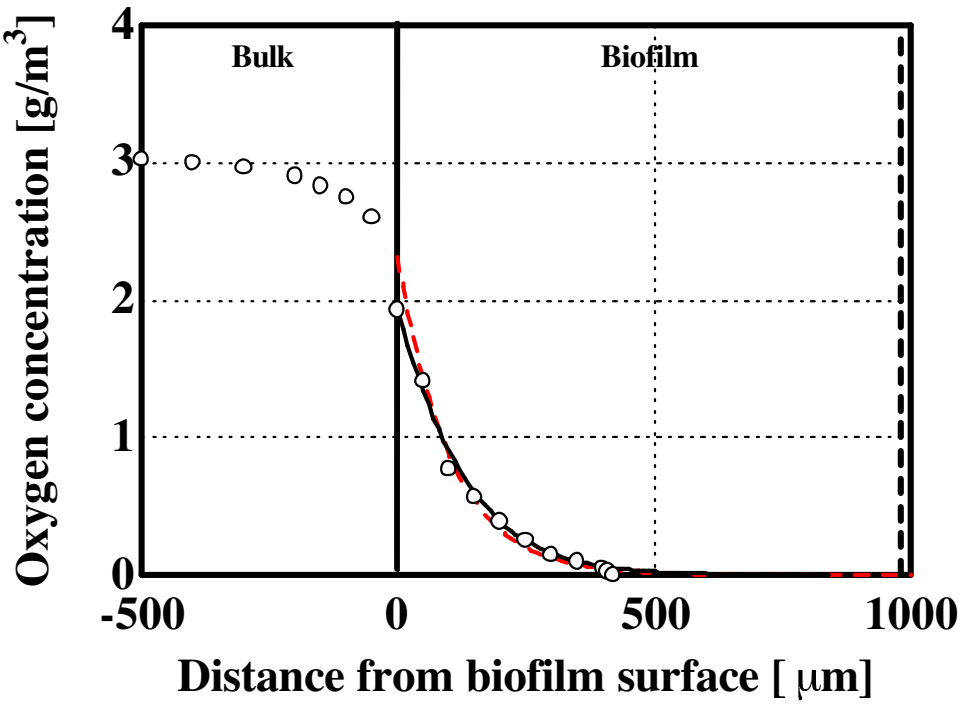


(b)

**Figure 3.6 Distribution of oxygen concentration inside biofilms of (a) 425 $\mu$m and (b) 980 $\mu$m thicknesses (open circles: experimental data from microelectrode analysis; broken line: fitted curve for exponential equation; continuous line: simulated curve)**

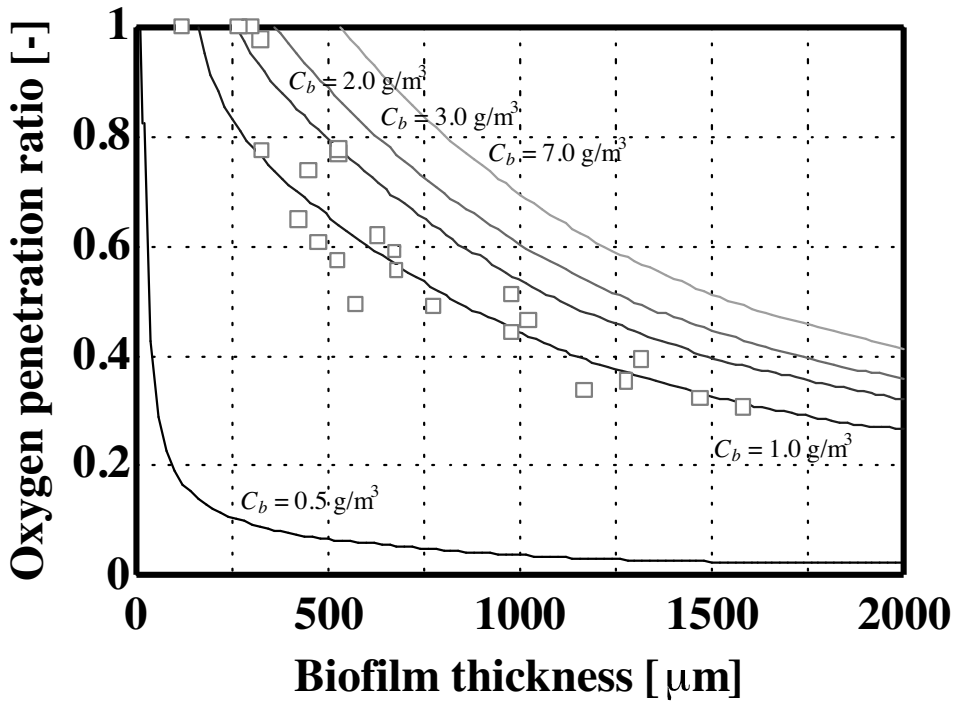


**Figure 3.7 Plots of oxygen penetration ratio against biofilm thickness for experimental data obtained at an oxygen concentration of 1.46 – 2.23 g/m$^3$ at the biofilm surface. Simulated curves are drawn for oxygen concentrations of 0.5 (---), 1.0 (- ), 2.0 (- ), 3.0 (- ) and 7.0 (- ) g/m$^3$ at the biofilm surface**

## 3.5 NOMENCLATURE

$a_1$ experimental coefficient (-)
$a_2$ experimental coefficient (-)
$a_3$ experimental coefficient (-)
$A$ experimental coefficient (-)
$C$ oxygen concentration (g/m$^3$)
$C_0$ oxygen concentration at carrier surface (g/m$^3$)
$C_s$ oxygen concentration at biofilm surface (g/m$^3$)
$C_b$ oxygen concentration at bulk (g/m$^3$)
$D_e$ effective diffusion coefficient of oxygen (m$^2$/s)
$D_f$ diffusion coefficient of oxygen inside biofilm (m$^2$/s)
$D_w$ diffusion coefficient of oxygen in water (m$^2$/s)
$J_f$ oxygen Flux inside biofilm (g/(m$^2$·s))
$J_w$ oxygen Flux at bulk (g/(m$^2$·s))
$k$ reaction constant (1/s)
$K_m$ monod saturated constant (g/m$^3$)
$t$ time (s)
$x$ distance from carrier surface (m)
$x_s$ distance at biofilm surface (m)
$X$ biofilm density (g/m$^3$)
$d$ biofilm thickness (m)

# Chapter IV

## STEP CHANGE ANALYSIS

**Observation of substrate concentration profile inside biofilm in step change analysis**

## 4.1 INTRODUCTION

In this chapter, step change in inlet substrate concentration represented by substrate was introduced into the completely mixed three-phase fluidized bed biofilm reactor. Substrates are total organic carbon (TOC), ammonium-ion ($NH_4^+$-N), nitrite-ion ($NO_2^-$-N), nitrate-ion ($NO_3^-$-N) and dissolved oxygen (DO). Furthermore, oxygen concentrations inside biofilm at each times were measured by original fabricated oxygen microelectrode. The purpose is to study the conditions inside biofilm during dynamic response. The step changes of 2 times and quarter times larger cases were conducted.

## 4.2 STEP UP CHANGE OF SUBSTRATE CONCENTRATION

### 4.2.1 MATERIALS AND METHODS

At start-up, the biofilm-attaching CB particles were washed to remove the excess sludge. The inlet TOC concentration of all the reactors was about 400 g/m$^3$ at the flow rate of 0.006 m$^3$/h. This concentration was chosen because this concentration and flow rate was known to allow continuous concentration operation of reactors maintain a stable biofilm structure but avoid excessive production of suspended sludge. Concentration of substrates was measured until steady-state values were obtained. Once the steady state was attained, twice step change in inlet concentration was introduced into the system. The concentrations inside the reactor at the start of the step change analysis are summarized in Table 4.1. After the step-up change of inlet concentration, the substrate concentration, which was considered as the state variables, were measured until new steady-state level was attained.

**Table 4.1 Step-up change in substrate concentration g/m$^3$**

| | TOC | $NH_4^+$-N |
|---|---|---|
| Before change | 200 | 50 |
| After change | 400 | 100 |

## 4.2.2 RESULTS AND DISCUSSION

The results of water quality analysis are shown in Figure 4.1. When the inlet substrate concentration is suddenly doubled, the concentration of the substrate inside the reactor increases due to accumulation. TOC (Figure 4.1. (a)) was increased from 0 hour, was attained to the peak at 25 hours. The accumulated substrate is gradually consumed until the rate of increase due to accumulation equals substrate consumption by the biomass. Thus, the peak is generated. After, the peak, substrate consumption becomes greater than the accumulation, and consequently the concentration inside the reactor goes down until a new steady-state condition, the inflow of substrate into the reactor is balanced by the biomass substrate utilization and the outflow of substrate with the effuent. The steady state of TOC was approached after 25 hour. This phenomenon was most popular in the step change experiments.

Next, some biofilm samples were get from the fluidized reactor at -2, 0, 3, 6, 9, 12, 20, 24, 29, 40, 51, 102 hours. The distribution of oxygen concentration inside a biofilm was measurement by microelectrode for each biofilm sample. The results of oxygen distribution are shown in Figure 4.2. The distribution of oxygen concentration inside the biofilm (DOCB) was increased until 6 hour. The DOCB wasn't changed from at 6 hours to at 20 hours. This term was the condition of most low oxygen concentration.

Time courses of the penetration depth of oxygen concentration inside the biofilm (PDOCB) and the oxygen concentration in the bulk (ODB) are shown in Figure 4.3. The PDOCB was like two peas in a pod with the ODB.

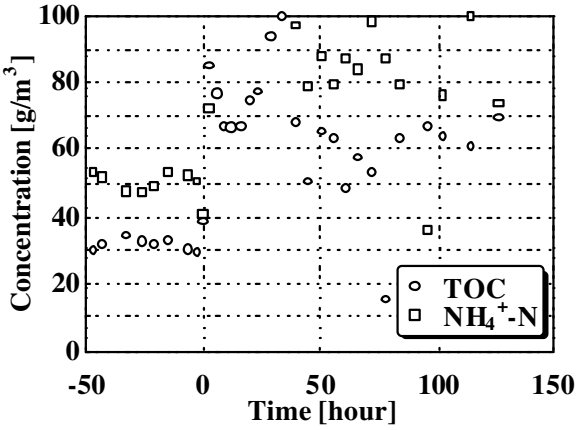


(a) TOC and $NH_4^+$-N

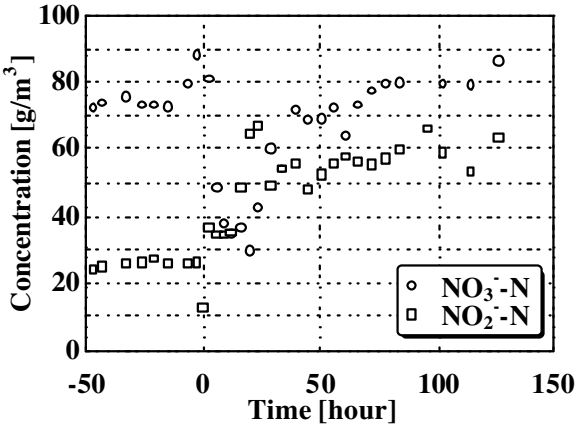


(b) $NO_x^-$-N

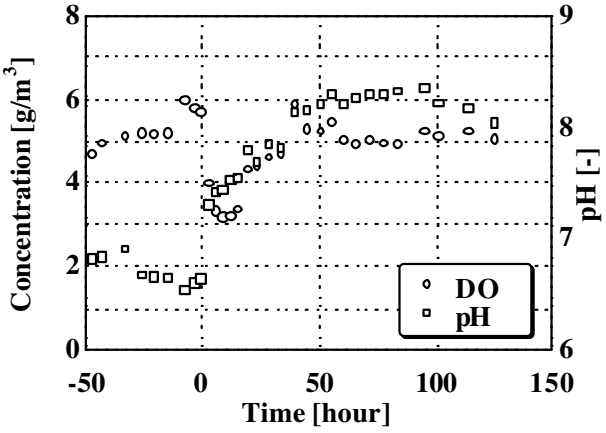


(c) DO and pH

**Figure 4.1. Time course of substrate concentration and pH in fluidized bed biofilm reactor at step-up change analysis**

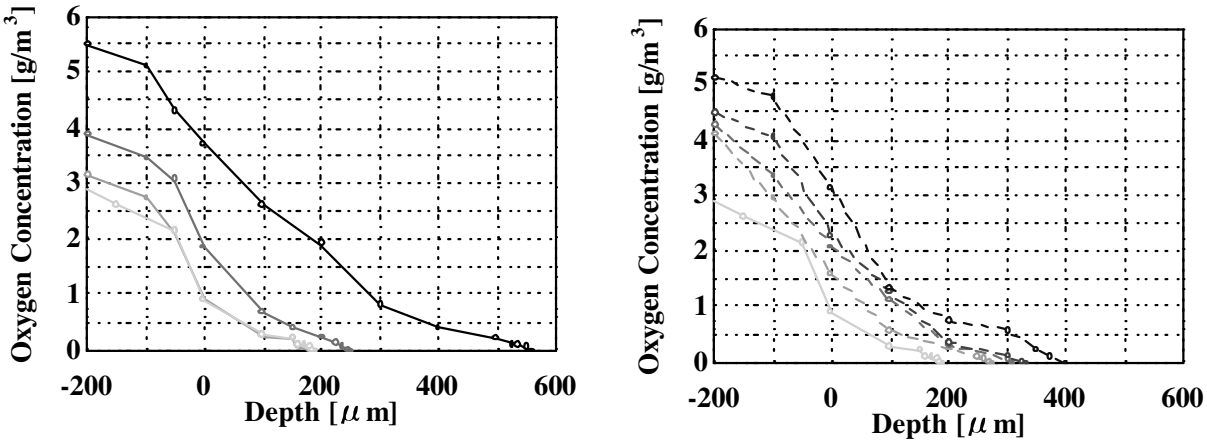


**Figure 4.2. Oxygen concentration profile inside biofilm at step-up change analysis**

## 4.2.3 CONCLUSIONS

It could be successful that the distribution of oxygen concentration inside the biofilm by oxygen microelectrodes in the step change analysis. As a result, the distribution of oxygen concentration inside the biofilm was influenced by the oxygen concentration in the bulk.

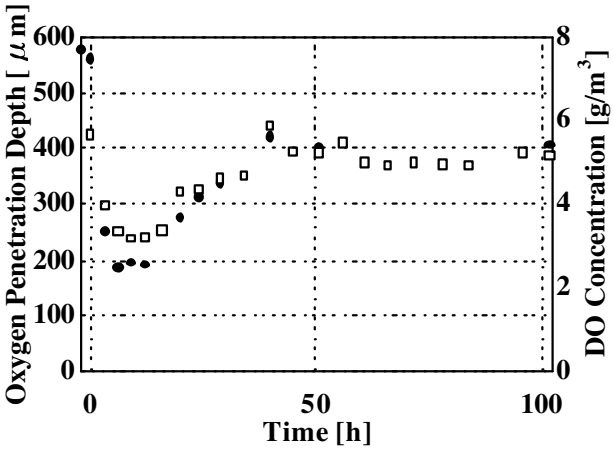


**Figure 4.3. Relationship between oxygen penetration depth and DO concentraion in bulk solution at step-up analysis**

# 4.3 STEP DOWN CHANGE OF SUBSTRATE CONCENTRATION

## 4.3.1 MATERIALS AND METHODS

The experiments to down inlet substrate concentration were conducted using biofilm sample which have no nitrifying activation by oxygen rate controlling. In this case, the recovery of nitrifying activities could be monitored. The substrate concentration and microprofile inside biofilm were determined. Two reactors were run, 1) RUN1: biofilm thickness is 120 $\mu$m, package rate is 20 % and 2) RUN2: biofilm thickness is 1200 $\mu$m,

package rate is 20%.

A complete-mixing three-phase fluidized bed reactor was used for continuous nutrient oxidation. After the steady state was confirmed, the inlet substrate concentrations were stepped down.

**Table 4.2 Step-down change in substrate concentration g/m$^3$**

| | TOC | $NH_4^+$-N |
|---|---|---|
| Before change | 400 | 100 |
| After change | 40 | 10 |

## 4.3.2 RESULTS AND DISCUSSION

Figure 4.4 shows the time courses of water quality and Figure 4.5 shows the distribution of oxygen concentration inside the biofilm. First, in the case of RUN1 (biofilm thickness = 120 $\mu$m), the biofilm had a nitrifying activity after the step change. Therefore, they had nothings before the step change. Because of the oxygen was penetrated inside the biofilm after step change, the oxygen concentration was nearly zero before the step change. The biofilms were released from oxygen rate controlling to decrease the substrate concentrations in the bulk solution at the 2.5 hours after. Consequently, oxygen existed inside biofilm and penetrated until 30 $\mu$m from biofilm-bulk interface into the biofilm. At the time, we suggested that the ammonia-oxidizing bacteria were existed in the region between 0 to 30 $\mu$m from the surface to the bottom of biofilm because nitrite-ion existed in the bulk. Figure 4.6 shows the image of FISH analysis. As a result, NSO190 probes (targeting an ammonia-oxidizing bacteria) were mainly reacted in the area between 0 to 30 $\mu$m in the biofilm. We found that ammonia-oxidizing bacteria inside biofilm can have activity, if very small quantity of oxygen penetrates into the biofilm.

Oxygen completely penetrates until particle which is the bottom part of biofilm at 4 and 6 hours after. In this case, oxygen concentration inside the biofilm was low. Therefore, two factors are suggested because nitrite-ion was not oxidized. First reason is the necessity of higher oxygen concentration is for nitrite-oxidization bacteria, second reason is the delay of responds for nitrite-oxidization bacteria forward an environmental change.

Furthermore, oxygen concentration was over 1 g/m$^3$ in the bottom area of biofilm at 8 hour. A whole biofilm condition was completely aerobic and nitrification smoothly proceeded.

Next, nitrification could not conducted by oxygen controlling before step change in the case that the biofilm thickness is 1200 $\mu$m. The oxygen concentration in the bulk was nearly zero. After step change, also oxygen was not penetrated into the biofilm at 4 hour.

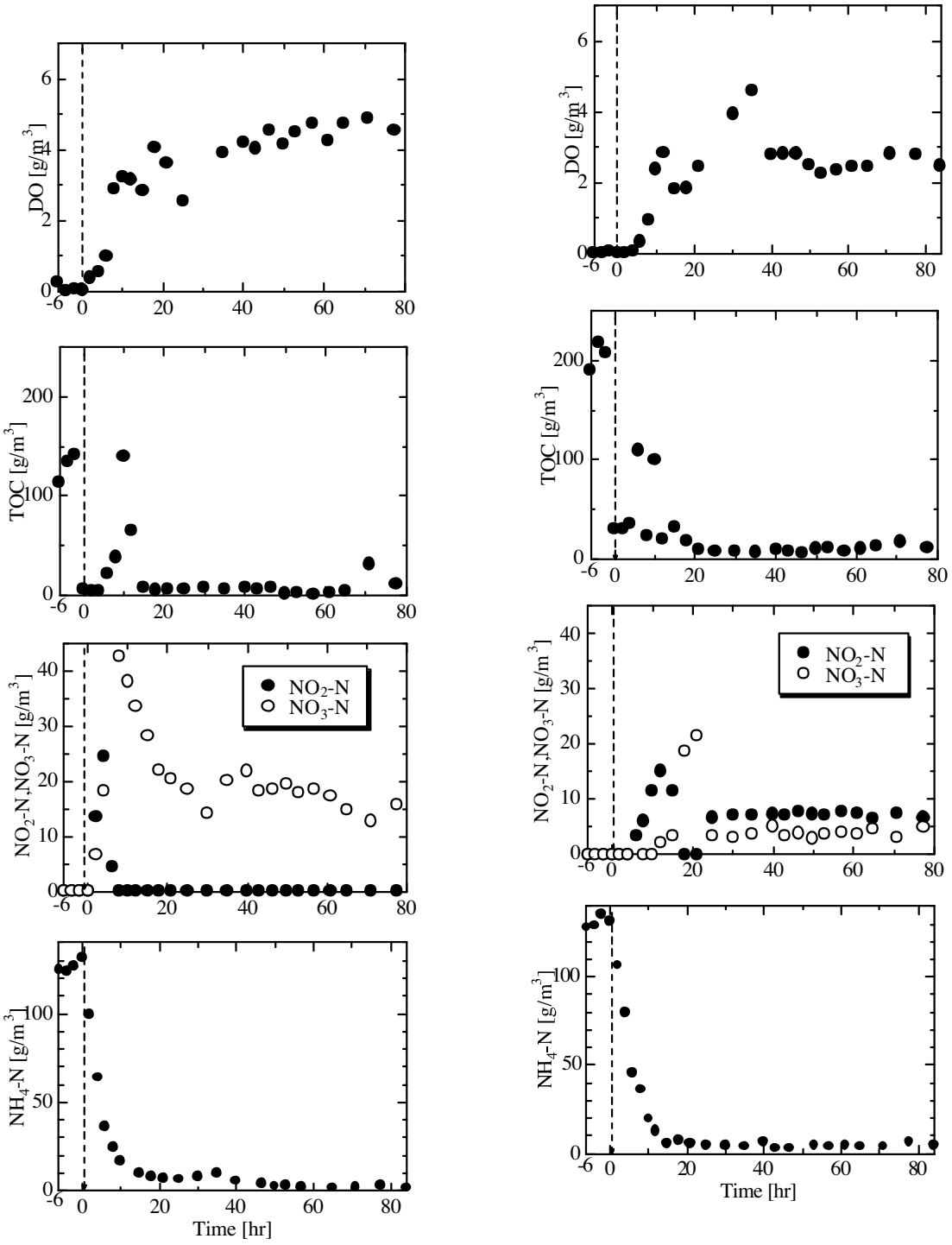


(a) RUN1 - Biofilm thickness: 120 $\mu$m

(b) RUN2 - Biofilm thickness: 1200 $\mu$m

**Figure 4.4 Time course of wastewater concentration in fluidized bed biofilm reactor at step-down change analysis**

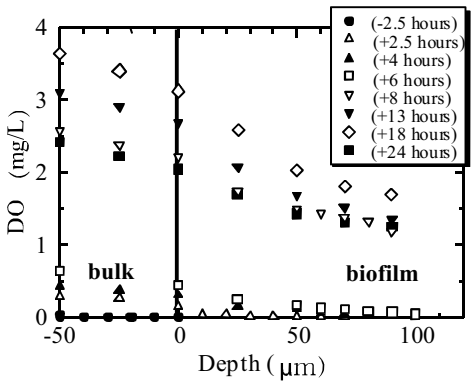


(A) Biofilm thickness:120 μm

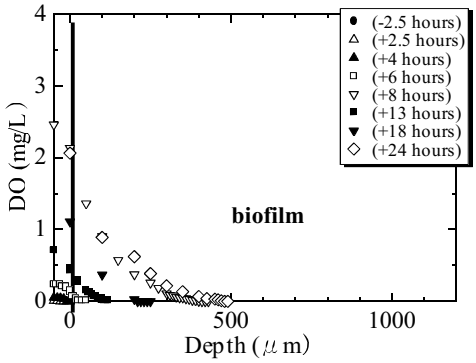


(B) Biofilm thickness: 1200 μm

**Figure 4.5 Concentration profile of DO inside biofilm**

## 4.3.3 CONCLUSION

It could be successful that the distribution of oxygen concentration inside the biofilm by oxygen microelectrodes in the step change analysis. As a result, the distribution of oxygen concentration inside the biofilm was influenced by the oxygen concentration in the bulk. Oxygen completely penetrates until particle which is the bottom part of biofilm.

# Chapter V

## NEW NITROGEN REMOVAL SYSTEM

**Simultaneous Nitrification and Denitrification by Controlling Vertical and Horizontal Microenvironment in a Membrane-Aerated Biofilm Reactor**

## 5.1 INTRODUCTION

In this chapter, we attempt the simultaneous nitrification and denitrification in a single reactor using MABR. First, adhesivities and biofilm formation of nitrifying bacteria onto the unmodified membrane and the membrane modified with grafted polymer chains were compared by observation of images taken by microscopy. Second, oxygen transfer rate from grafted membrane was measured. Third, the microbial and physical properties inside the biofilm in MABR with a complex microbial population were monitor ed using microelectrodes and the FISH method. In addition, the contribution of the change in the microbial population in the vertical direction, as a result of plug flow (from the bottom to the top of the reactor), to nitrification efficiency is verified by reaction rate constants which are mathematically determined using the ammonium nitrogen profiles inside the biofilm.

## 5.2 EVALUATION OF BACTERIAL ATTACHMENT

### 5.2.1 MATERIAL AND METHODS

#### 5.2.1.1 Surface modification of membrane

We used two types of membranes: one is an original polyethylene membrane, the other is a surface-modified polyethylene membrane. The latter was prepared by the radiation-induced graft polymerization (RIGP) method as described by Tsuneda *et al*. [66]. A commercially available polyethylene membrane (Asahi Chemical Industry Co.) was used as the base polymer for grafting. A vinyl monomer, glycidyl methacrylate (GMA), was grafted onto the polyethylene membrane by applying the RIGP method. The degree of GMA grafting (dg), defined by Eq. (1), was set at 72%:

$$dg = \{(W_1 - W_0)/W_0\} \times 100\ [\%] \qquad (1)$$

where $W_0$ and $W_1$ are the weights of unmodified and GMA-grafted membranes, respectively. Next, the GMA-grafted membrane was reacted with diethylamine for the introduction of diethylamino (DEA) groups. The amount of introduced DEA groups was evaluated to measure the ion-exchange capacity by titration. The DEA-grafted membrane was used as the surface-modified membrane.

The surface characteristics of these membranes were evaluated by measuring the effective charge density. The effective charge density was obtained by fitting the experimental results to the equation based on the Donnan equilibrium and the Nernst-Planck equation using membrane potential. Membrane potential measurement was carried out according to Higa *et al*. [86]. There were two cells divided by the membrane. The membrane area was $9.4\times10^{-2}$ $m^2$. The concentration of KCl electrolyte solution on one side was ten times higher than that on the other side. The potential was measured at 20°C using glass electrodes, which we originally fabricated, with a salt bridge (3 *M* KCl).

### 5.2.1.2 Wastewater treatment system

The above-described substrate (600 g-N/$m^3$) was continuously fed at 1.0 L/day to a fluidized bed bioreactor with an effective volume of 2 L. The unmodified and modified membranes were used as supporting materials on which biofilms were immobilized. The temperature was maintained at 30℃. Air was supplied to the reactor at a suitable rate to fully disperse the biofilms and to provide excess dissolved oxygen. The pH of the solution in the reactor was adjusted to 7.5-8.0 by the addition of 1 *M* NaOH 1-3 times a day.

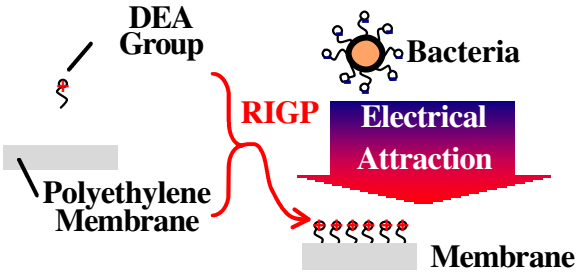


**Fig.5.1 Schematics Diagram of Adhesion Between Bacteria and Membrane**

### 5.2.1.3 Method of water quality analysis

All culture samples were filtered through a 0.2-$\mu$m-pore-size membrane filter (Isopore®, Millipore Co.) prior to water quality measurement. The amount of organic pollutants was evaluated as total organic carbon (TOC) with an automatic TOC analyzer (TOC-500, Shimadzu Co.). Ammonium-nitrogen ($NH_4^+$-N) was determined using an ammonia-selective electrode (F-203, Horiba Co., Japan). Nitrite-nitrogen ($NO_2^-$-N) and nitrate-nitrogen ($NO_3^-$-N) were determined using an ion-chromatograph system (IC-Anion-PW, UV-8011, Tosoh Co.). Biofilm thickness was calculated from the image obtained by optical microscopy (BH-2, Olympus Co.). Bacterial adhesion to membranes was confirmed from SEM (S-2500, Hitachi Co.) images.

## 5.2.2 RESULTS AND DISCUSSION

### 5.2.2.1 Surface properties of membrane

The difference in surface properties of the unmodified and modified membranes is summarized in Table 5.1. The grafted membrane carried 26 times more positive charges than the unmodified membrane because a large amount of diethylamino groups (3.5 mol/kg) was successfully introduced to the membrane by the grafting method.

**Table 5.1 Surface properties of original and grafted membrane**

| | Original | Grafted(dg=72%) |
|---|---|---|
| Ion-exchange capacity [mol/kg] | - | +3.5 |
| Effective charge density [mol/$m^3$] | +23.5 | +625 |

**Table 5.2 Membrane Characteristics**

| Properties | Plane | Grafted |
|---|---|---|
| Thickness [mm] | 0.15 | |
| Pore Size [$\mu$m] | 0.2 | |
| Porosity [%] | 70 | |
| DEA group Density [mol/kg T-P] | 0 | 3.08 |

### 5.2.2.2 Adhesivity of nitrifying bacteria

The surfaces of the unmodified and modified membranes which had been fluidized in the flask for 14 days were observed by SEM (Figure 5.2). It was found that the microorganisms hardly attached to the unmodified membrane, whereas many rod-shaped microorganisms such as nitrifying bacteria adhered to the grafted membrane in 14 days. From this result, the bacterial adhesivity was proved to be strongly influenced by the positive charge and the polymer brush which had been introduced by the radiation-induced grafting method.

### 5.2.2.3 Ammonium-nitrogen removal efficiency

Membranes with nitrifying biofilm were introduced into a fluidized bed bioreactor where $NH_4^+$ as a nutrient was continuously fed. The results of water quality analysis are shown in Figure 2.6. Biofilm thickness was observed every day by optical microscopy. Representative images of biofilms on the membranes are shown in Figure 5.3.

The thickness of biofilm on the grafted membrane was approximately 20 $\mu$m at day 88 and approximately 100 $\mu$m at day 150. In contrast, no biofilm was formed on the unmodified membrane. Therefore, a new supporting material suitable for biofilm formation was successfully developed by modification of the surface by the grafting method. Nitrification rate was very unstable until day 50 because of the small amount of attached and suspended nitrifying bacteria. However, after day 50, a thick biofilm was retained, and

thus the $NH_4^+$-N removal rate reached as high as 0.3 kg-N/($m^3$·day) and became stable.

#### 5.2.2.4 Ammonium-nitrogen removal rate

The $NH_4^+$-N removal rate of the biofilm on the grafted membrane was computed for comparison with that of the biofilm on the cement ball (CB) in the bioreactor where ammonia-rich inorganic wastewater was continuously fed. We assumed that all biofilm samples and reactor conditions were maintained at steady states, and computed the $NH_4^+$-N removal rates on the basis of two different series of data: 1. bulk concentration change, 2. concentration profile inside the biofilm.

##### *5.2.2.4.1 Bulk concentration change*

The $NH_4^+$-N removal rates per unit biofilm surface area were calculated from Eq. (2) based on mass balance of inlet and outlet concentrations.

$$R_A = \frac{F\left(C_{IN} - C_{OUT}\right)}{S_B} \qquad (2)$$

Here, $R_A$ is $NH_4^+$-N removal rate per unit biofilm surface area, $F$ is flow rate, $C_{IN}$ is $NH_4^+$-N concentration at inlet and $C_{OUT}$ is $NH_4^+$-N concentration at outlet. The biofilm surface area ($S_B$) on the membrane was calculated from the biofilm thickness determined by using light microscope on the assumption that the biofilm uniformly adhered, and from the number of membrane put into the reactor at start up. The shape of membrane with biofilm was regarded as a rectangular parallelepiped. Similarly, the biofilm surface area on the CB was calculated from the biofilm diameter and the number of CB inside the reactor. The shape of CB with biofilm was regarded as a sphere. The calculated $S_B$ values for the membrane and for the CB were 0.26 and 90 $m^2$, respectively. Then, $R_A$ was computed using the average of all $C_{IN}$ and $C_{OUT}$ data in the steady state.

##### *5.2.2.4.2 Concentration profile inside the biofilms*

The $NH_4^+$-N removal rates per unit biofilm surface area were calculated from Eq. (3) based on Fick's law of the profiles inside the biofilms.

$$R_A = D_A \cdot \frac{\partial C_A}{\partial X} = -J_A \qquad (3)$$

Here, $C_A$ is $NH_4^+$-N concentration, $D_A$ is $NH_4^+$ diffusion coefficient, $X$ is distance from the biofilm surface and $J_A$ is flux. The $NH_4^+$-N profile inside the biofilm approximately exhibited exponential function with respect to the distance from the interface between biofilm and bulk. Thus, $R_A$ was computed from the $NH_4^+$-N flux at biofilm surface. In this calculation, $NH_4^+$ diffusion coefficient in pure water at 20℃ ($D_A$=1.38×$10^{-9}$ $m^2$/day) was used [87].

The computed results are summarized in Table 5.3. The $NH_4^+$-N removal rates obtained from the concentration profile inside the biofilm were lower than those obtained from the bulk concentration change. This is mainly because the latter inevitably include the

contribution of suspended nitrifying bacteria. Consequently, the former, which had been evaluated by the microelectrode method, were suitable for the estimation of the exact nitrification rate of the biofilm. Okabe *et al*. (1999) reported that the $NH_4^+$-N removal rate computed using the concentration profile inside the biofilms in a rotating disk reactor (RDR) was $2.7\times10^{-2}$ g-N/($m^2$·day) [18]. On the other hand, Araki *et al*. (1999) and Sumino *et al*. (1998) reported that the values computed using bulk concentration changes in fluidized bed bioreactors with nitrifying bacteria entrapped by high-molecular-weight polymers were $9.6\times10^{-2}$ and $4.0\times10^{-2}$ g-N/($m^2$·day), respectively [88, 89]. Therefore, we have obtained biofilms with highly efficient nitrification rates in this study.

**Table 5.3 The $NH_4^+$-N removal rates unit biofilm surface area of the biofilms**

| | | $NH_4^+$-N removal rates [g-N/($m^2$·day)] | |
|---|---|---|---|
| | | From bulk conc. change | From conc. profile inside the biofilms |
| This study | Membrane | 2.3 | 1.0 |
| | CB | $7.0\times10^{-3}$ | $5.0\times10^{-3}$ |
| Okabe *et al*. (1999) | RDR | - | $1.7\times10^{-3}$ |
| Araki *et al*. (1999) | entrapped | $9.6\times10^{-2}$ | - |
| Matsumura *et al*. (1998) | entrapped | $4.0\times10^{-2}$ | - |

## 5.2.3. CONCLUSIONS

Nitrifying bacteria exhibited high adhesivities to the membrane whose surface had been modified with positively charged graft polymer chains, and nitrifying biofilms with sufficient thickness were obtained within a short time.

## 5.2.4. NOMENCLATURE

*C* : Concentration [g/$m^3$]
*D* : Diffusion coefficient [$m^2$/day]
*dg* : Degree of GMA grafting [%]
*F* : Flow rate [$m^3$/day]
*J* : Flux [g/($m^2$·day)]
*R* : $NH_4^+$-N removal rate [g/($m^2$·day)]
*S* : Surface area [$m^2$]
*W* : Membrane weight [g]
*X* : Distance from the biofilm surface [m]

Subscripts:
*0* : Polyethylene membrane

*1* : GMA-grafted membrane
*A* : Ammonium-nitrogen
*B* : Biofilm
*IN* : Inlet
*OUT* : Outlet


(a) (b)

**Figure 5.2 SEM picture of membrane surface at day 14 (×3000). (a) original membrane, (b) grafted membrane**

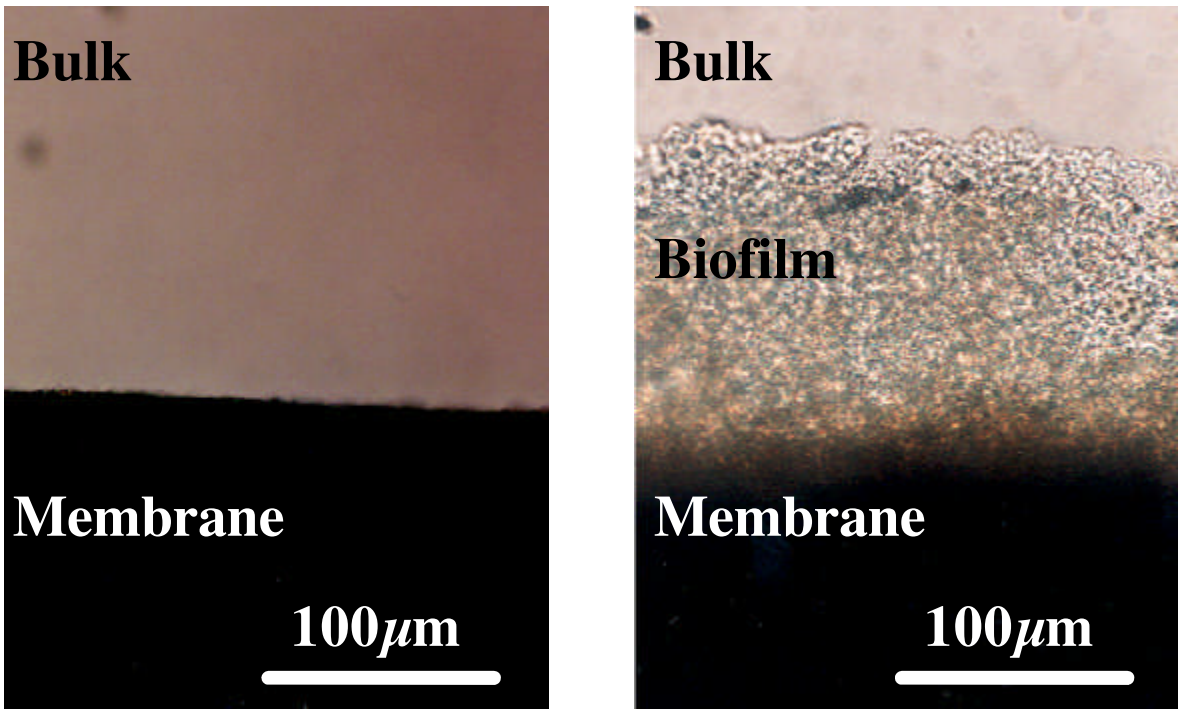


(a) (b)

**Figure 5.3 Microscopic picture of membrane with biofilm at day 150 (×100) . (a) original membrane, (b) grafted membrane**

# 5.3 OXYGEN TRANSFER RATE FROM THE MEMBRANE

## 5.3.1 MATERIALS AND METHODS

### 5.3.1.1 Membrane Properties

A hollow fiber membrane (Asahi Chemical Industry) made of polyethylene was used for biofilm-supporting material. The length was 20 cm, the inside and outside diameters were 1.9 and 3.0 mm, respectively, being the pore size was 0.3 $\mu$m. The membrane has positive charges on the surface after the introduction of diethylamino groups by radiation-induced graft polymerization (RIGP) (Tsuneda *et al*., 1998). Our previous work (Hibiya *et al*., 1999) confirmed that adhesion of nitrifying bacteria to the membrane can be greatly enhanced by this surface modification technique.

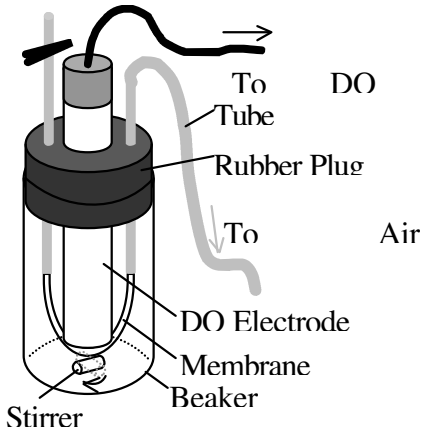


**Figure 5.4 Schematic of Measuring System on Oxygen Transfer Rate**

**Table 5.4 Membrane Characteristic**

| | |
|---|---|
| Diameter [mm] | 3 |
| Thickness [mm] | 0.15 |
| Length [mm] | 200 |
| Pore Size [$\mu$m] | 0.2 |
| DEA group Density [mol/Kg T-P] | 3.08 |

## 5.3.2 RESULTS AND DISCUSSION

### 5.3.2.1 Oxygen Transfer Rate

The relationship between intramembrane pressure and oxygen transfer rate to a bulk solution was measured, as the amount of intramembrane-supplied oxygen is most important in the design of the MABR. The DO electrode and the hollow-fiber membrane, which was connected to a pure air cylinder, were inserted into an airtight beaker. After pure water with a low concentration of DO was injected into the beaker, the DO concentration in the bulk was measured for a certain time, maintaining a constant pressure. Figure 5.5 shows that the amount of oxygen transferred is proportional to air pressure, which indicates that it is possible to control the DO concentration in the MABR equipment by adjusting the air pressure. Moreover, when the domestic modified wastewater used in this experiment was completely oxidized under an aerobic condition though the reactions of $C + O_2 = CO_2$ and $NH_4^+ + 2O_2 = NO_3^- + H_2O + 2H^+$. The relation presented the oxygen transfer rate of 0.06 g/day was required. Thus, the air pressure in the following experiments with the MABR was determined to be set at 10 kPa according to Figure 5.5.

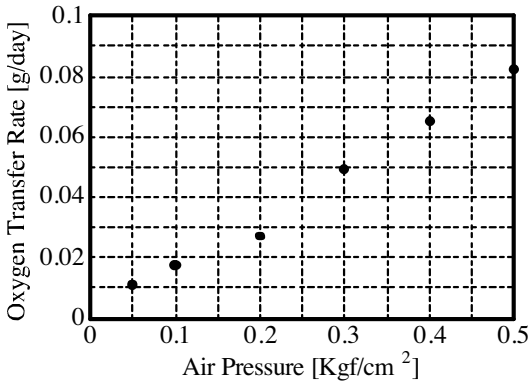


Figure 5.5 Relationship between Air Pressure and Oxygen Transfer Rate

### 5.3.3 CONCLUSION

The air pressure in the following experiments with the MABR was determined to be set at 10 kPa from the experimental result, as The relation presented the oxygen transfer rate of 0.06 g/day was required.

## 5.4 Development of membrane aeration biofilm reactor

### 5.4.1 MATERIAL AND METHODS

#### 5.4.1.1 Bioreactor Configuration

The MABR system is schematically depicted in Figure 5.7. The cylindrical reactor made of polycarbonate has an effective volume of 100 $cm^3$. Three surface-modified hollow-fiber membranes were inserted to create a specific surface area of 57 $m^2/m^3$. The domestic modified wastewater to be supplied (TOC: 100 $g/m^3$, $NH_4^+$-N: 25 $g/m^3$) consisted of glucose (250 $g/m^3$), $KH_2PO_4$ (8.0 $g/m^3$), $K_2HPO_4$ (16 $g/m^3$), $(NH_4)_2SO_4$ (118 $g/m^3$), $MnCl_2 \cdot 4H_2O$ (200 $g/m^3$), $MgSO_4 \cdot 7H_2O$ (300 $g/m^3$), $CaCl_2 \cdot 2H_2O$ (2.0 $g/m^3$), $NaMoO_4 \cdot 2H_2O$ (100 $g/m^3$) and Fe(III)-EDTA (10 $g/m^3$). This wastewater was supplied to the bottom of the reactor by a peristaltic pump at a flow rate of $4 \times 10^{-4}$ $m^3$/day. Pure air was supplied to one end of the hollow-fiber membrane from a gas cylinder under the intra membrane pressure of 10 kPa. The other end of the hollow-fiber membrane was sealed with a stopper. The temperature was kept at $30 \pm 0.5$ °C. The seed sludge was obtained from a reactor which had been run with the domestic modified wastewater for a one month. Initially, the reactor was filled with the feed solution and the seed sludge without continuous feeding. Then, continuous feeding started after the organic carbon concentration in the reactor fell below 25 $g/m^3$.

#### 5.4.1.2 Analytical Method

All culture samples were filtered through a 0.2-$\mu$m-pore-size membrane filter (Isopore®,

Millipore) prior to water quality measurement. The amount of organic pollutants was evaluated as the amount of total organic carbon (TOC), using an automatic TOC analyzer (TOC-500, Shimadzu). The ammonium-nitrogen ($NH_4^+$-N) concentration was determined using an ammonia-selective electrode (F-203, Horiba). The nitrite-nitrogen ($NO_2^-$-N) and nitrate-nitrogen ($NO_3^-$-N) concentrations were determined using an ion-chromatograph system (IC-Anion-PW, UV-8011, Tosoh). The dissolved oxygen (DO) concentration was determined using a diaphragmal electrode (DOL-10, DKK) and pH was measured using a glass electrode (TPX-90, Toko Chemical Laboratries). The biofilm thickness was calculated from an image obtaining using an optical microscope (BH-2, Olympus).

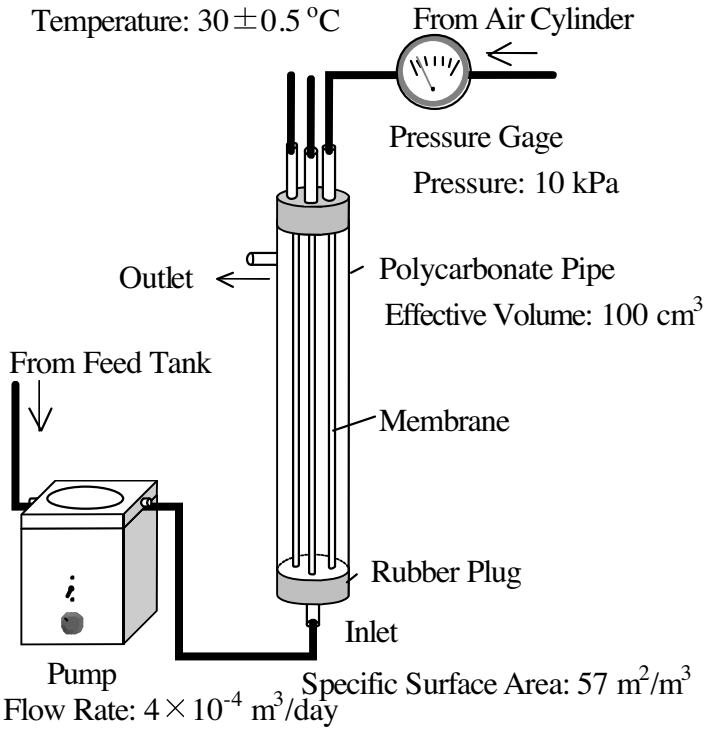


**Figure 5.7 Schematic diagram of the MABR used in this study**

### 5.4.1.3 Microelectrode

Microelectrodes for pH, $NH_4^+$ and $NO_3^-$ were prepared as described by de Beer *et al.* (1997). Soda lime glass tubes with 1-mm-diameter (100 $\mu$L Micropipetts, Drummond) were drawn into microcapillaries using a micropipette puller (MPT-1, Shimadzu). The tip diameter was about 5-7 $\mu$m for all LIX microelectrodes and the tips of the electrodes were silanized with 20% (v/v) solution of trimethylchlorosilane in carbon tetrachloride to obtain a hydrophobic surface for optimal adhesion of the LIX membranes. After the tips of the microelectrodes were filled with the silanized solution, the electrodes were baked for at least 1 h at 130ºC to remove traces of water. The liquid membrane used was 10% (wt/wt) tridodecylamine and 1% (wt/wt) sodium tetraphenylborate in 2-nitrophenyloctyl ether for pH microelectrode and 10% (wt/wt) nonactine and 1% (wt/wt) sodium tetraphenylborate in

2-nitrophenyloctyl ether for the $NH_4^+$ microelectrode. The electrolytes used were 0.04 *M* $KH_2PO_4$, 0.023 *M* NaOH and 0.015 *M* NaCl for the pH microelectrode and 0.01 *M* $NH_4Cl$ for the $NH_4^+$ microelectrode. To measure the spatial distributions inside the biofilms, pH, $NH_4^+$ and $NO_3^-$ microelectrodes were inserted into the biofilm samples at 10 $\mu$m intervals using a micromanipulator (MMO-203, Narishige). The biofilm were fixed on a glass plate that was filled with a solution obtained from the reactor. The measurements were immediately conducted without air supply from membrane.

#### 5.4.1.4 Fluorescence In Situ Hybridization (FISH)

All Biofilm and suspended sludge samples for FISH analysis were immediately fixed with 4% paraformaldehyde. The biofilm sample was dispersed to individual cells by ultrasonication, and placed in a hybridization well on a gelatin-coated microscopic slide. For hybridization of the biofilm and sludge samples on the slide, the standard hybridization protocol described by Amann (1995) was used. Two 16S rRNA-targeted oligonucleotide probes were used for *in situ* detection of ammonia-oxidizing and heterotrophic bacteria: 1) NSO190 (labeled with TRITC, indicated as red in figures): specific for the region of the 16S rRNA of all ammonia-oxidizing bacteria of the $\beta$-subclass of proteobacteria (Mobarry *et al*., 1996); 2) EUB338 (labeled with Cy5, indicated as blue in figures): a probe for targeting all eubacteria (Amann *et al*., 1990b). After hybridization, the biofilm samples on slides were examined with a confocal laser-scanning microscope (TCS NT, Leica).

## 5.4.2 RESULTS AND DISCUSSION

### 5.4.2.1 Water Quality

Time courses of water quality (TOC, $NH_4^+$-N, $NO_2^-$-N and $NO_3^-$-N) are shown in Figure 5.8. The effluent TOC concentration in the initial stage (days 0-30) fluctuated from 5 to 25 g/m$^3$. Removal proceeded further at day 30; the average value was about 1 g/m$^3$. In contrast, nitrogen compounds were rapidly removed in the initial stage at day 0-5. Here, it is worth noting that nitrification occurred even though the DO concentration in the bulk was lower than 0.5 g/m$^3$. This result indicates that sufficient oxygen was supplied to the biofilm through the hollow-fiber membrane. Moreover, removal efficiencies of TOC and T-N are shown in Figure 5.9. It is confirmed that 90% removal of TOC and T-N from the domestic modified wastewater (carbon load: 0.42 kg-C/(m$^3$·day) and nitrogen load: 0.16 kg-N/(m$^3$·day)) could be attained consistently by using the MABR for 150 days. The less dense biofilm with 50-300 $\mu$m thickness was formed over the entire surface of the hollow-fiber membane.

### 5.4.2.2 Microprofile inside Biofilm

The microprofiles were obtained from three different positions in the vertical direction: a

low point, a central point and an upper point of the reactor. In order to minimize the error, the measurements were performed three times at each point. The average results are shown in Figure 5.10. $NH_4^+$-N was almost completely removed from the lower part to the central part of the reactor. Negligible $NO_3^-$-N was detectable throughout the whole reactor. This phenomenon can be explained as follows: 1) $NO_3^-$ reduction occurred immediately after $NO_3^-$ was produced by nitrification, 2) $NO_2^-$ was directly reduced to $N_2$ gas without changing to $NO_3^-$.

On the other hand, the existence of nitrifying bacteria was directly observed using the FISH method. The biofilm and the suspended sludge in the lower part of the reactor were taken as samples. The *in situ* observation of the biofilm sample could not be accomplished because the biofilm density was too low to retain its original formation throughout the pretreatment process of FISH analysis. Therefore, the biofilm sample was observed after dispersion to individual cells by ultrasonication. Figure 5.11 (a) shows that the microbial species inside the biofilm of the lower part were mostly ammonia-oxidizing bacteria. Nitrite-oxidizing bacteria was not detected by FISH method using the probes of NIT3 (Nitrobacter) and NSR1156 (Nitrospira) (data not shown). This might be due to the following two reasons. 1) Nitrite-oxidizing bacteria have a higher oxidation rate unit a cell compared with ammonia-oxidizing bacteria (*Nitrosomonas*: 0.9-20 fmol/cell/h, *Nitrobacter*: 5.1-42 fmol/cell/h (Prosser *et al*., 1989)). 2) Main reaction is a shortcut reaction without passing through a nitrate-ion. Suzuki *et al*. (2000) evaluated the activities of nitrification and denitrification inside the biofilm for the MABR by means of a batch test after extracting a biofilm sample. They reported that the profiles of the microbial species in the inner and the outer sides of the biofilm were clearly separated and the denitrifying bacteria mainly existed in outer side of the biofilm. However, in this study, although the FISH method could not be applied for the samples of the inner and outer sides of the biofilm separately, the ratio of ammonia-oxidizing existing bacteria inside the biofilm was significantly high. It is generally thought that since both of the batch experiment and the MPN method are not in situ measurements, the existence ratios of different types of bacteria can not be evaluated accurately by those methods. In particular, in the case of bacteria with a fast growth rate, such as denitrifying bacteria, their population might be overestimated.

When the FISH method was applied to the suspended sludge, ammonia-oxidizing bacteria were scarcely observed, as shown in Figure 5.11 (b). This result indicates a high possibility that the bacteria existing in the suspended sludge were species of denitrifying bacteria because the DO concentration was very low and organic carbon sources existed in the bulk. The exists of denitrifying bacteria in the sludge were confirmed by a batch experiment crosschecked. Furthermore, when the FISH method was also applied to the biofilm samples of the central and upper parts of the reactor, the same results as for the lower part were obtained (data not shown).

### 5.4.2.3 Evaluation of Nitrification Rate

The spatial distributions inside the biofilm determined using microelectrodes were theoretically analyzed and the kinetic parameters were calculated. The modeling method was adopted under the following three assumptions: 1) steady state inside the biofilm, 2) first-order kinetics of the biological reaction, 3) validity of the dimensions of the cylinder (because the length of the hollow-fiber membrane was much longer than the biofilm thickness). The mass balance equation inside the biofilm can be expressed as follows.

$$D_A \cdot \frac{1}{r} \cdot \frac{d}{dr} \cdot \left( r \cdot \frac{dC_A}{dr} \right) = k_1 \cdot C_A \qquad \text{Eq. 1}$$

This equation was solved under the following boundary condition (Eq. 2). Here, $I_0$ and $K_0$ are the Bessel functions.

$$\begin{cases} r = r_b, C_A = C_b \\ r = r_m, C_A = C_m \end{cases} \qquad \text{Eq. 2}$$

$$C_A = A \cdot I_0\left( \sqrt{\frac{k_1}{D_A}} \cdot r \right) + B \cdot K_0\left( \sqrt{\frac{k_1}{D_A}} \cdot r \right) \qquad \text{Eq. 3}$$

where

$$A = \frac{C_b \cdot K_0\left( \sqrt{\frac{k_1}{D_A}} \cdot r_m \right) - C_m \cdot K_0\left( \sqrt{\frac{k_1}{D_A}} \cdot r_b \right)}{I_0\left( \sqrt{\frac{k_1}{D_A}} \cdot r_b \right) \cdot K_0\left( \sqrt{\frac{k_1}{D_A}} \cdot r_m \right) - I_0\left( \sqrt{\frac{k_1}{D_A}} \cdot r_m \right) \cdot K_0\left( \sqrt{\frac{k_1}{D_A}} \cdot r_b \right)} \qquad \text{Eq. 4}$$

$$B = \frac{C_b - A_1 \cdot I_0\left( \sqrt{\frac{k_1}{D_A}} \cdot r_b \right)}{K_0\left( \sqrt{\frac{k_1}{D_A}} \cdot r_b \right)} \qquad \text{Eq. 5}$$

The empirical ammonium-nitrogen profiles inside the biofilm were fitted using Eq. 3 that is to the solution of the mass balance equation inside the biofilm. The calculated values of $k_1/D_A$ are summarized in Table 5.5. In these cases, the diffusion coefficient in the biofilm, $D_A$, was unknown. Thus, $D_A$ was calculated using the ammonium-nitrogen flux to the biofilm. The mass balance of the bulk solution in the reactor can be expressed by Eq. 6.

$$J_A = \frac{Q}{S_b} \cdot (C_{in} - C_{out}) \qquad \text{Eq. 6}$$

When the average values of ammonium-nitrogen inlet and outlet concentrations at days 50-150, the biofilm surface area and the flow rate were substituted into Eq. 6, the nitrification rate of the biofilm surface area, $J_A$, was obtained as 0.77 g-N/($m^2$·day).

On the other hand, Fick's first law can be defined as Eq. 7.

$$J_A = D_A \cdot \frac{dC_A}{dr} \qquad \text{Eq. 7}$$

The slope of ammonium-nitrogen concentration at the outside surface of the biofilm was obtained by the curve empirically fitted to the microelectrode data. The relationship between the slope at the biofilm surface and the vertical position in the reactor is shown Figure 5.12. The exponential equation was empirically fitted for the relation between the slope at the biofilm surface and the distance from the bottom of the reactor. Integrating the exponentially fitted curve from the bottom to the top of the reactor, the representative value of the slope of ammonium-nitrogen concentration at the biofilm surface was calculated as $dC_A/dr = 3.2\times10^4$ g-N/m$^4$. The diffusion coefficient, $D_A$, inside the biofilm was obtained as $2.4\times10^{-5}$ m$^2$/day by substituting two representative values, $J_A$ = 0.77 g-N/(m$^2$·day) and $dC_A/dr = 3.2\times10^4$ g-N/m$^4$, into Eq. 7. Finally, the rate constants for the first-order reaction, $k_1$, at each point of the reactor were calculated, as summarized at the bottom of Table 5.5.

The $k_1$ value obtained for the upper point was significantly smaller than those at the other points. This result indicated that the ammonia-oxidizing bacteria species existing at the upper point was different from those at other points. Moreover, substituting the calculated diffusion coefficient into Eq.7, the nitrification rates at each point were determined. As a result, the nitrification rates at the lower, central and upper points were 3.0, 0.41 and $2.3\times10^{-2}$ g-N/(m$^2$·day), respectively. The nitrification rate at the lower point was 7 and 125 times larger than those at the central and upper points, respectively, which confirmed that the microbial population gradient in the vertical direction was successfully created by a plug flow configuration.

**Table 5.5 Summary of mathematically analyzed values for first-order reaction**

| | At lower point | At central point | At upper point | Representation |
|---|---|---|---|---|
| $k_1/D_A$ [1/m$^2$] | $1.0\times10^8$ | $9.1\times10^7$ | $2.0\times10^7$ | |
| $J_A$ from Eq.6 [g-N/(m$^2$·day)] | | | | 0.77 |
| $dC_A/dx$ [g-N/m$^4$] | $1.2\times10^5$ | $1.7\times10^4$ | $9.6\times10^2$ | $3.2\times10^4$ |
| $D_A$ [m$^2$/day] | | | | $2.4\times10^{-5}$ |
| $k_1$ [1/day] | $2.5\times10^3$ | $2.2\times10^3$ | $5.0\times10^2$ | |
| $J_A$ from Eq.7 [g-N/(m$^2$·day)] | 3.0 | 0.41 | $2.3\times10^{-2}$ | |

## 5.4.3. CONCLUSION

1. The simultaneous nitrification and denitrification of domestic modified wastewater (carbon load: 0.42 kg-C/(m$^3$·day) and nitrogen load: 0.16 kg-N/(m$^3$·day)) was successfully carried out by controlling the oxygen supply condition.
2. The pH, $NH_4^+$ and $NO_3^-$ concentration distributions inside the biofilm were measured using microelectrodes. Ammonium ions are transferred from the lower part to the central part of the reactor, and negligible nitrate was detected throughout the reactor.

3. The FISH method was applied to the biofilm and the suspended sludge in the MABR. Habitat segregation between ammonia-oxidizing bacteria and other bacteria was verified. The ammonia-oxidizing bacteria were mainly distributed inside the biofilm, and other bacteria, including denitrifying bacteria, were mainly distributed over the suspended sludge.
4. The ammonium-nitrogen distributions inside the biofilm, which were measured using microelectrodes, were theoretically analyzed and the kinetic parameters were calculated. Consequently, the experimental data were found to be fitted by a first-order reaction, and nitrification rates at lower, central and upper points were 3.0, 0.41 and $2.3\times10^{-2}$ g-N/($m^2$·day), respectively.

## 5.4.4 NOMENCLATURE

*A* Integral coefficient [-]
*B* Integral coefficient [-]
*C* Concentration [g/$m^3$]
*D* Diffusion coefficient [$m^2$/day]
*I* Bessel function [-]
*J* Flux [g/($m^2$·day)]
*k* Reaction rate constant [1/day]
*K* Bessel function [-]
*Q* Flow rate [$m^3$/day]
*r* Radius distance [m]
*S* Surface area [$m^2$]

subscript
*0* Zero order
*1* First order
*A* Ammonium-nitrogen
*b* Outside surface of biofilm
*in* Inlet
*out* Outlet
*m* Outside surface of membrane

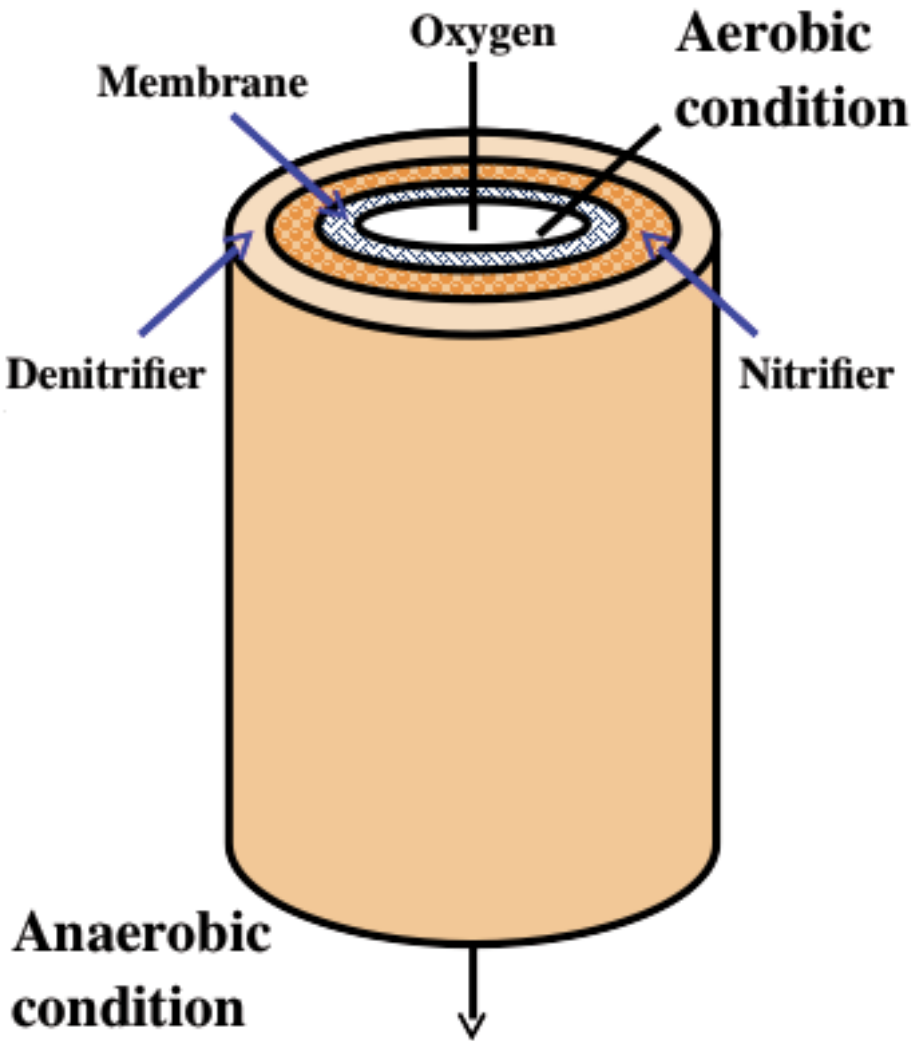


**Figiure 5.6 Image of membrane aeration biofilm reactor**

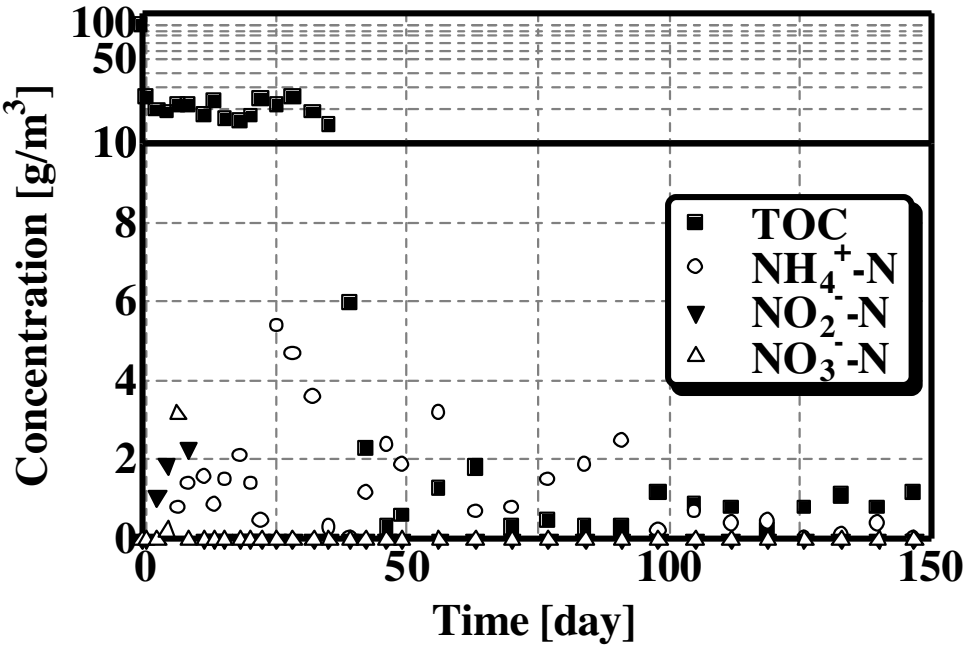


**Figure 5.8 Time courses of water quality of TOC (■), $NH_4^+$-N (○), $NO_2^-$-N (▼) and $NO_3^-$-N (△) in the effluent of the MABR**

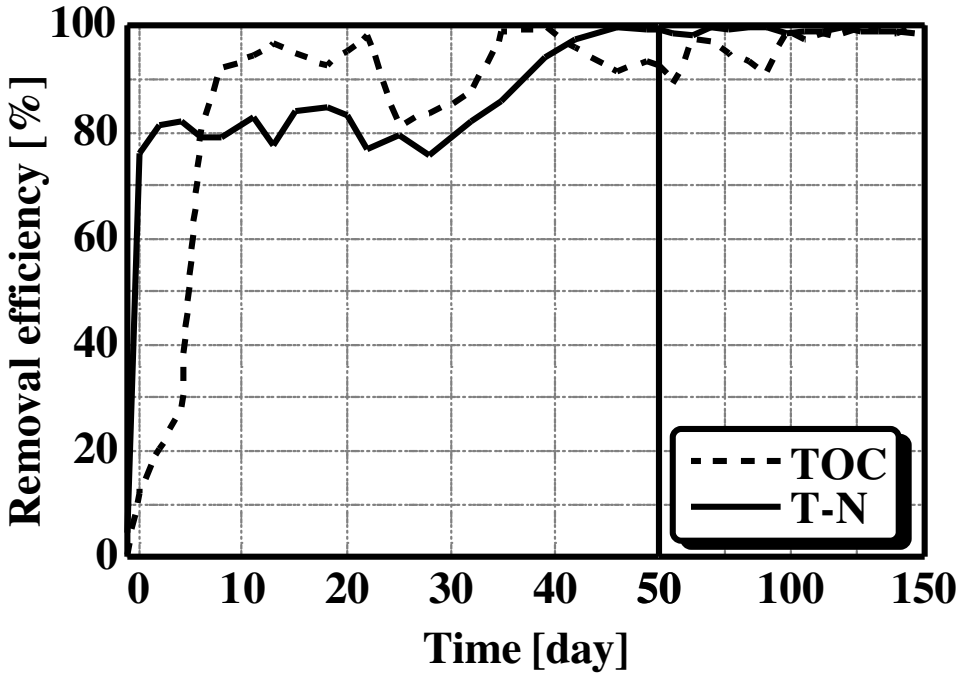


**Figure 5.9 Time courses of removal efficiency of carbon (---) and nitrogen (- ) components**

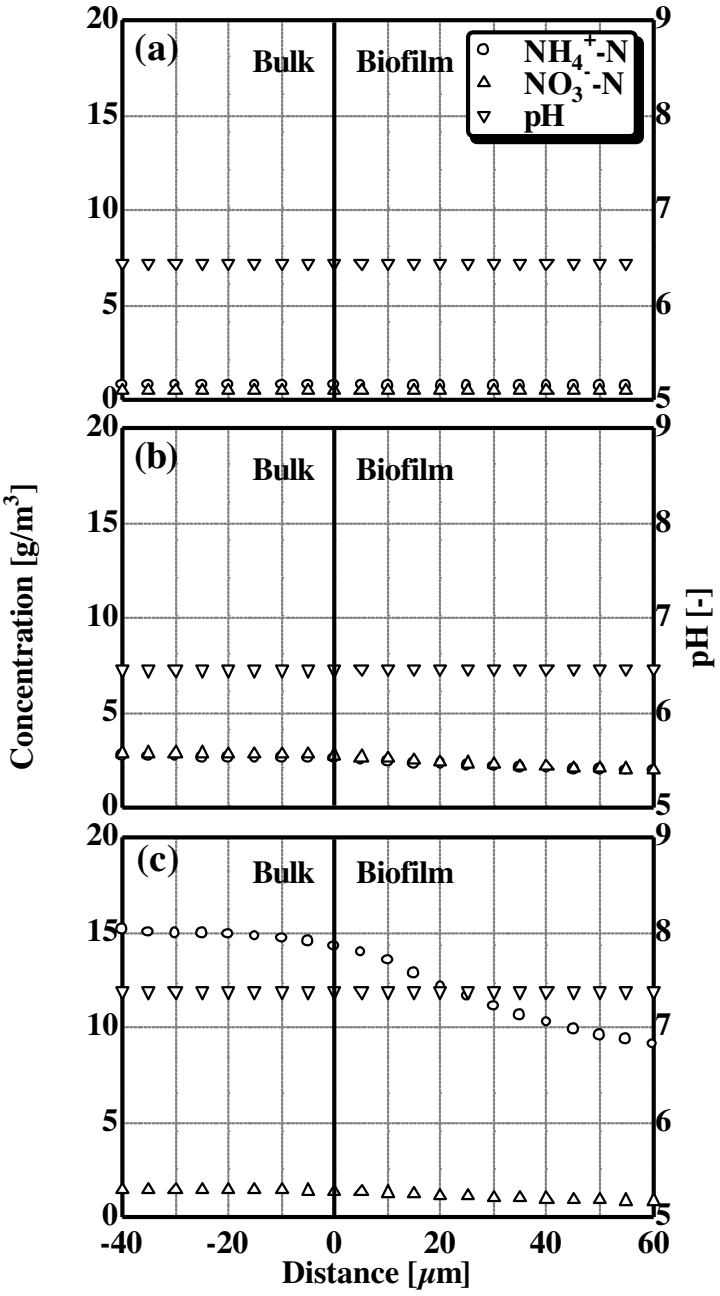


**Figure 5.10 Distributions of $NH_4^+$-N (?), $NO_3^-$-N (△) and pH (▽) concentrations inside the biofilm (a) at upper point, (b) at middle point and (c) at under point in MABR at day 144**

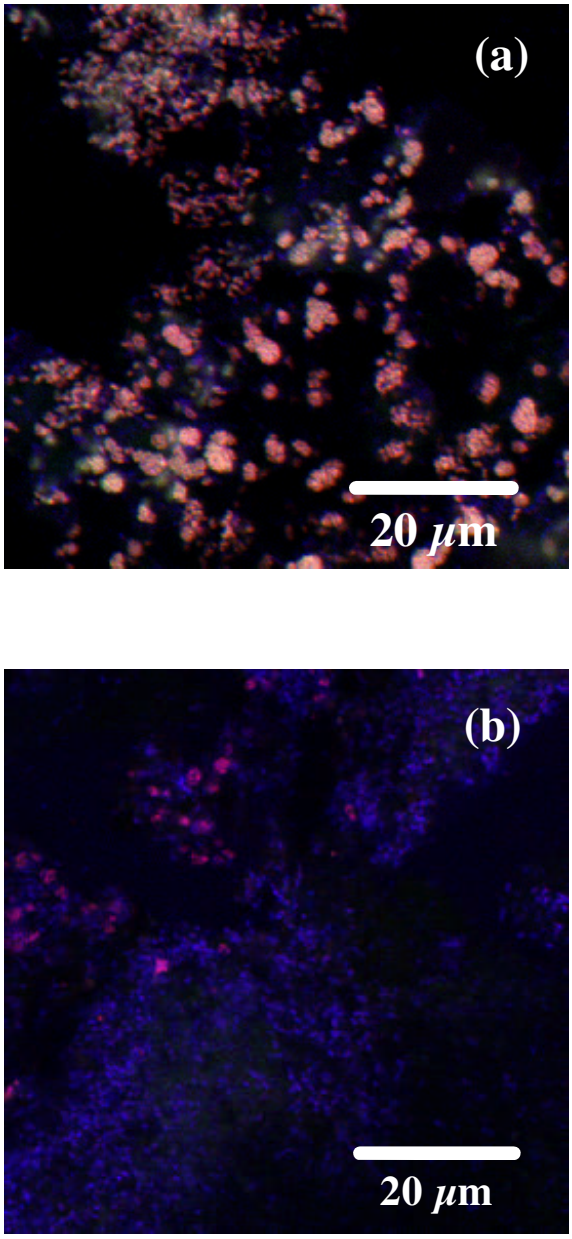


**Figure 5.11 Microbial habitations of the ammonia-oxidizing bacteria and the other bacteria inside the reactor monitored by FISH analysis in (a) a biofilm and (b) a suspended sludge. The Ammonia-oxidizing bacteria shows pink (NSO190) and the other bacteria shows blue (EUB338)**

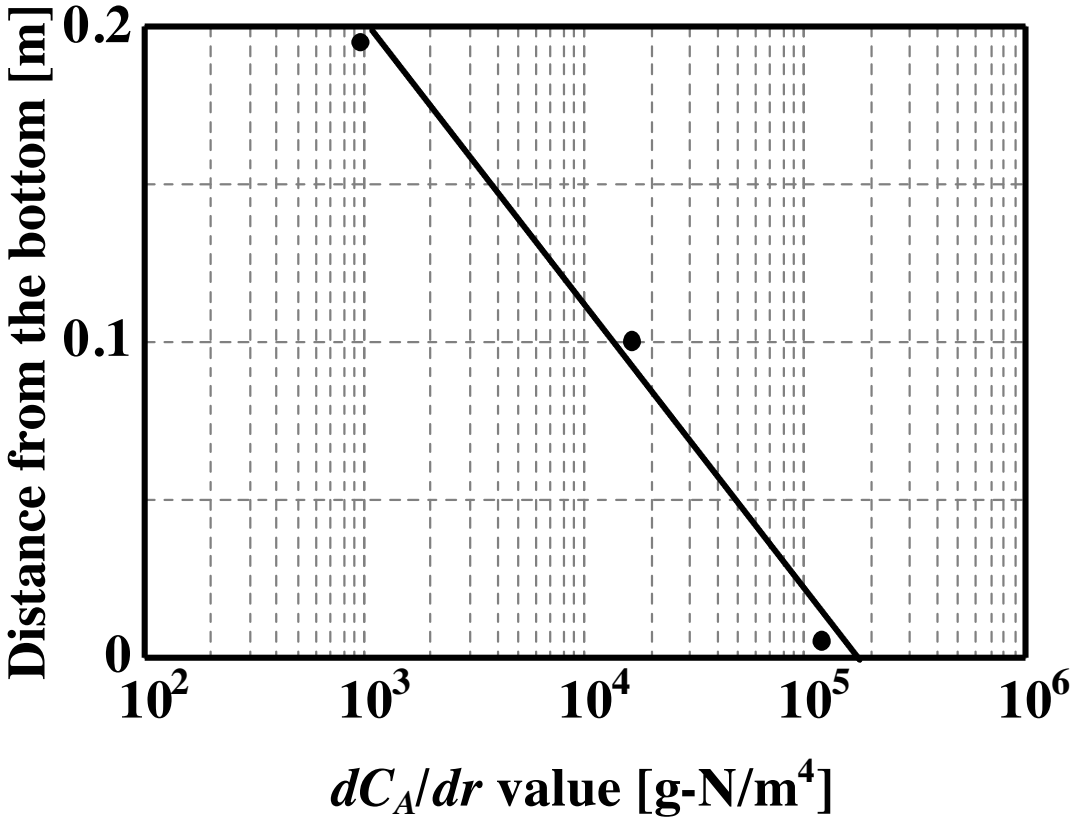


**Figure 5.12 Relationship between d$C_A$/d$r$ value and position in the reactor**

# Chapter VI

## CONCLUSION AND PERSPECTIVE

## 6.1 CONCLUSION

### 6.1.1 Determination and simulation of oxygen distribution inside biofilm

The distribution of oxygen in a biofilm is very important in oxidation processes such as simultaneous carbon oxidization and nitrification using a fluidized bed biofilm reactor. In this study, attention was paid to biofilm thickness and biofilm density which significantly affect the oxygen distribution in biofilms. Using an oxygen microelectrode that we fabricated, the oxygen distribution in biofilms of different thicknesses was measured, and subsequently oxygen penetration depth and ratio were determined. As a result, oxygen penetration ratio decreased gradually with increasing biofilm thickness. Moreover, the kinetic parameters of a Monod-type reaction and the effective diffusion coefficient were computed based on the oxygen distribution in the biofilms. Using the obtained biofilm dry density, kinetic parameters and effective diffusion coefficient, the oxygen distribution in biofilms was successfully fitted to the results of a microelectrode analysis. The oxygen distribution was simulated by the finite difference method using the kinetic parameters and effective diffusion coefficient. Therefore, oxygen penetration ratio can be predicted at various biofilm thicknesses and oxygen concentrations in a bulk solution.

### 6.1.2 Simultaneous nitrification and denitrification in single reactor

Nitrogen and carbon components in domestic modified wastewater were completely removed by simultaneous nitrification and denitrification using a membrane-aerated biofilm reactor (MABR) where biofilm was fixed on a hollow fiber membrane. To measure the spatial distribution of pH, ammonium and nitrate ions and to observe microbes inside the biofilm formed on the membrane, microelectrodes and a fluorescent in situ hybridization (FISH) method were applied. Due to plug flow in vertical direction (from the bottom to the top of the reactor), ammonium nitrogen was gradually removed, and negligible nitrate nitrogen was detected throughout the reactor. The FISH revealed that ammonia-oxidizing bacteria were mainly distributed inside the biofilm and other bacteria which included denitrifying bacteria were mainly distributed outside the biofilm and over the suspended sludge. In order to characterize bacterial activity in the vertical direction, the nitrification

rates at lower, central and upper points were calculated using microelectrode data. The nitrification rate at the lower point was 7 and 125 times higher than those at central and upper points, respectively. These results show that the removal of carbon and nitrogen compounds was accomplished efficiently by using various kinds of bacteria distributed vertically and horizontally in a single reactor.

## 6.2 PERSPECTIVE

The information in various kinds of biofilms, which has been regarded as a 'black-box', would be elucidated by use of microelectrode and FISH methods, allowing the development of a new microbial reaction system with controlled environment in the biofilm. Consequently, a new MABR will be introduced to the wastewater treatment system that requires removal of nitrogen compounds with a high efficiency.

# REFERENCES

## STUDY AND ACQUAINTANCE

[1] Tchobanoglous G. and Burton F.L. (1991) Advanced wastewater treatment. Wastewater engineering, treatment, disposal, and reuse. McGraw-Hill, Inc., Singapore, 711-726.

[2] Kuenen J.G. and Robertson L.A. (1988) Ecology of nitrification and denitrification. In J. A. Cole and S. J. Ferguson (ed.) The nitrogen and sulphur cycles. Cambridge University Press, Cambridge, 161-218.

[3] Hong W.Z., Donald S.M., William K.O. and Frederic A.K. (1999) Controlling factors for simultaneous nitrification and denitrification in a two-stage intermittent aeration process treating domestic sewage. Wat. Res. 33(4), 961-970.

[4] Menoud P., Wong C.H., Robinson H.A., Farquhar A., Barford J.P. and Barton G.W. (1999) Simultaneous nitrification and denitrification using siporaxTM packing. Wat. Sci. Technol. 40(4-5), 153-160.

[5] A. Hirata, M. Noguchi, Biological wastewater treatment by three-phase fluidization — characteristics and basic design method, Water Sci. Technol.. 30 (1994) 91-100.

[6] S. L. Safferman, P. L. Bishop, Aerobic fluidized bed reactor with internal media cleaning, J. Environ. Eng. 122 (1996) 284-291.

[7] A. Hirata, T. Takemoto, K. Ogawa, J. Auresenia, S. Tsuneda, Evaluation of kinetic parameters of biochemical reaction in three-phase fluidized bed biofilm reactor for wastewater treatment, Biochem. Eng. J. 5 (2000) 165-171.

[8] R. M. Worden, T. L. Donaldson, Dynamics of a biological fixed film for phenol degradation in a fluidized bed bioreactor, Biotechnol. Bioeng. 30 (1987) 398-412.

[9] K. D. Wisecarver, L. S. Fan, Biological phenol degradation in a gas-liquid fluidized bed reactor, Biotechnol. Bioeng. 33 (1989) 1029-1038.

[10] A. Hirata, C. Takahashi, M. Arai, Biological treatment of coke-oven wastewater in three-phase fluidized bed, Environ. Conservation Eng. 20 (1991) 183-192.

[11] A. Hirata, H. S. Lee, S. Tsuneda, T. Takai, Treatment of photographic processing wastewater using anaerobic-aerobic biofilm reactor, Water Sci. Technol.. 36 (1997) 91-99.

[12] Lewandowski Z., Lee W.C., Characklis W.G. and Little B. (1989) Dissolved oxygen and pH microelectrode measurements at water immersed metal surfaces. Corrosion, 45, 92-98.

[13] De Beer D., Schramm A., Santegoeds C.M. and Kuhl M. (1997) A nitrite microsensor for profiling environmental biofilms. Appl. Environ. Microbiol. 63(3), 973-977.

[14] Amann R.I., Binder J., Olson R.J., Chisholm S.W., Devereux R. and Stahl D.A.

(1990a) Combination of 16S rRNA-targeted oligonucleotide probes with flow cytometry for analyzing mixed microbial populations. Appl. Environ. Microbiol. 56, 1919-1925.

[15] Glockner F.O., Fuchs B.M. and Amann R.I. (1999) Bacterioplankton compositions of lakes and oceans: A first comparison based on fluorescence in situ hybridization. Appl. Environ. Microbiol. 65(8), 3721-3726.

[16] Brossa E.L., Mora R.R. and Amann R.I. (1998) Microbial community composition of wadden sea sediments as revealed by fluorescence in situ hybridization. Appl. Environ. Microbiol. 64(7), 2691-2696.

[17] Schramm A., Larsen L.H., Revsbech N.P. and Amann R.I. (1997) Structure and function of a nitrifying biofilm as determined by microelectrodes and fluorescent oligonucleotide probes. Wat. Sci. Technol. 36(1), 263-270.

[18] Okabe S., Satoh H. and Watanabe Y. (1999) In situ analysis of nitrifying biofilms as determined by in situ hybridization and the use of microelectrodes. Appl. Environ. Microbiol. 65(7), 3182-3191.

[19] C. M. Santegoeds, G. Muyzer, D. de Beer, Biofilm dynamics studied with microsensors and molecular techniques, Water Sci. Technol.. 37[4-5] (1998) 125-129.

[20] A. Schramm, L/ H. Larsen, N. P. Revsbech, N. B. Ramsing, R. I. Amann, K. H. Schleifer, Structure and function of a nitrifing biofilm as determined by in situ hybridization and use of microelectrode, Appl. Environ. Microbiol. 62 (1996) 4641-4647.

[21] D. de Beer, A. Schramm, C. M. Santegoeds, M. Kuhl, A nitrite microsensor for profiling environmental biofilms, Appl. Environ. Microbiol. 63 (1997) 973-977.

[22] Z. Lewandowski, Notes on biofilm porosity, Water Res.. 34 (2000) 2620-2624.

[23] Amann R.I., Krumholz L. and Stahl D.A. (1990b) Fluorescent oligodeoxynucleotide probing of whole cells for determinative, phylogenetic and environmental studies in microbiology. J. Bacteriol. 172, 762-770.

[24] G. Muyzer, N. B. Ramsing, Molecular methods to study the organization of microbial communities, Water Sci. Technol.. 32[8] (1995) 1-9.

[25] C. Picioreanu, M. C. M. van Loosdrecht, J. J. Heijnen, Mathmatical modeling of biofilm structure with a hybrid differential-discrete cellular automaton approach, Biotechnol. Bioeng. 58[1] (1998) 101-116.

[26] S. Okabe, Y. Oozawa, K. Hirata, Y. Watanabe, Relationship between population dynamics of nitrifiers in biofilms and reactor perfomance at various C:N ratios, Water Res.. 30 (1996) 1563-1572.

[27] Y. Aoi, T. Miyoshi, T. Okamoto, S. Tsuneda, A. Hirata, A. Kitayama, T. Nagamune, Microbial ecology of nitrifying bacteria in wastewater treatment process examined by fluorescence in situ hybridization, J. Biosci. Bioeng. 90[3] (2000) 234-240.

[28 T. C. Zhang, Y. C. Fu, P. L. Bishop, Competition in Biofilms, Water Sci. Technol.. 29[10-11] (1994) 263-270.

[29] C. Nicolella, M. C. M. van Loosdrecht, J. J. Heijnen, Identification of mass transfer parameters in three-phase biofilm reactor, Chem. Eng. Sci. 54 (1999) 3143-3152.

[30] J. Wimpenny, W. Manz, U. Szewzyk, Heterogeneity in biofilms, FEMS Microbiol. Rev. 24 (2000) 661-671.

[31] Williamson K. and McCarty P.L (1976) A model of substrate utilization by bacterial

films. Water Pollut. Control Fed. 48(1), 9-24.

[32] Harremoës P. (1978). Biofilm kinetics in: Water Pollution Microbiology. Mitchell (ed.) vol. 2, 71-109, Wiley, N.Y.

[33] Mueller J. A., Paquin P. and Famularo J. (1980). Nitrification in rotating biological rotators. Wat. Pollut. Control Fed., 52 (4), 688-710.

[34] Rittmann B. and McCarty P. (1980a). Model of steady state biofilm kinetics. Biotechnol. Bioeng., 22, 2343-2357.

[35] Rittmann B. and McCarty P. (1980b). Evaluation of steady state biofilm kinetics. Biotechnol. Bioeng., 22, 2359-2373.

[36] Kissel J.C., McCarty P.L. and Street R. L. (1984). Numerical simulation of mixed culture biofilm. J. Env. Engin., 110(2), 393-412.

[37] Wanner O and Reichert P. (1996). Mathematical modelling of mixed-culture biofilms. Biotechnol. Bioeng., 49(2), 172-184.

[38] Rittmann B. E. and Manem, J. A. (1992). Development and experimental evaluation of a steady-state, multispecies biofilm model, Biotechnol. Bioeng., 39, 914-922.

[39]Lewandowski Z., Stoodley P., Atobelli S. and Fukushima E. (1994). Hydrodynamics and kinetics in biofilm systems-recent advances and new problems. Wat. Sci. Tech., 29(1011), 223-229.

[40] Zhang T.C. and Bishop P.L. (1994). Density, porosity and pore structure of biofilms. Wat. Res., 28(11), 2267-2277.

[41] Bishop P. (1997). Biofilm structure and kinetics. Wat. Sci. Tech., 36(1), 287-294.

[42] Wanner O. and Gujer, W. (1986). A multispecies biofilm model, Biotechnol. Bioeng. 28, 314-328.

[43] Rauch W., Vanhooren H. and Vanrolleghem P. (1998). A simplified mixed-culture biofilm model. Wat. Res., 39(9), 2148-2162.

[44] Holmberg A. and Ranta J. (1982). Procedures for parameter and state estimation of microbial growth process models. Automatica. 18(2), 181-193.

[45] Fink D. J., Na T.Y. and Schults J.S. (1973). Effectiveness factor calculations for immobilized enzyme catalyst. Biotechnol. Bioeng., 15,879-888.

[46] Grady C. P. L., Daigger G., and Lim H. C. (1999). Biological Wastewater Treatment 2nd ed., Marcel Dekker Inc. New York, USA.

[47] Saez P., Rittmann, B. (1988). Improved pseudoanalytical solutions for steady-state biofilm kinetics. Biotechnol. Bioeng., 32, 379-385.

[48] Heath M. S., Wirtel S. A. and Rittmann B. E. (1990). Simplified design of biofilm process using normalized loading curves. Research Journal, Water Pollution Control Federation, 62, 185-192.

[49] Rittmann B. E., Crawford L., Tuck C. and Namkung E. (1986). In situ determination of kinetic parameters for biofilms: isolation and characterization of oligotrophic biofilms. Biotechnol. Bioeng., 28, 1753-1760.

[50] Borse. G.J., (1997). Numerical Methods with MATLAB, PWS Publishing Company, Boston MA.

[51] Reichert P.(1994). AQUASIM, a tool for simulation and data analysis for aquatic systems, Wat. Sci Tech. 30(2), 21-30.

[52] Horn H. and Hempel D.(1996). Substrate utilization and mass transfer in an autotrophic biofilm system: experimental results and numerical simulation. Biotechnol. Bioeng., 53(4), 363-371.

[53] Horn H. and Hempel D. (1997). Growth and decay in an auto/heterotrophic biofilm. Wat. Res., 31(9), 2242-2252.

[54] A. Hirata, T. Takemoto, K. Ogawa, J. Auresenia, S. Tsuneda, Evaluation of kinetic parameters of biochemical reaction in threephase fluidized bed biofilm reactor for wastewater treatment, Biochem. Eng. J. 5 (2000) 165–171.

[55] W.T. Tang, K. Wisecarver, L.S. Fan, Dynamics of a draft tube gas–liquid–solid fluidized bed bioreactor for phenol degradation, Chem. Eng. Sci. 42 (1987) 2123–2134.

[56] J. Auresenia, K. Hibiya, S. Tsuneda, A. Hirata, Kinetic equation for simultaneous oxidation of total organic carbon and ammonium–nitrogen in three-phase fluidized bed biofilm reactor, in: Proceedings of the IAWQ Conference on Biofilm System, 1999, in CD-ROM.

[57] W.C. Ying, A.E. Humphrey, Biophysicochemical adsorption model systems for wastewater treatment, J. Water Pollut. Con. Fed. 51 (1979) 2661–2667.

[58] G.F. Andrews, C. Tien, Bacterial film growth on adsorbent surface, AIChE J. 27 (1981) 396–403.

[59] S.C.P. Wang, C. Tien, Bilayer film model for interaction between adsorption and bacterial activity in granular activated carbon columns, AIChE J. 30 (1984) 786–801.

[60] R.M. Worden, T.L. Donaldson, Dynamics of a biological fixed film for phenol degradation in a fluidized-bed bioreactor, Biotechnol. Bioeng. 30 (1987) 398–412.

[61] A. Hirata, Y. Hosaka, H. Umezawa, Characteristics of simultaneous utilization of oxygen and substrate in a three-phase fluidized bed bioreactor, J. Chem. Eng. Jpn. 23 (1990) 303–307.

[62] A. Hirata, M. Noguchi, Biological wastewater treatment by three-phase fluidization—characteristics and basic design method, Water Sci. Technol. 30 (1994) 91–100.

[63] A.W. Decho, G.R. Lopez, Exopolymer microenvironments of microbial flora: multiple and interactive effects on trophic relationships, Limnol. Oceanogr. 38 (1993) 1633–1645.

[64] C. Freeman, M.A. Lock, The biofilm polysaccharide matrix: a buffer against changing organic substrate supply, Limnol. Oceanogr. 40 (1995) 273–278.

[65] W. Lee, K. Saitoh, S. Furusaki and T. Sugo, Biotechnol. Bioeng., 53 (1997) 523.

[66] Tsuneda S., Saito K., Furusaki S., Sugo T. and Ishigaki I. (1992). Water/acetone permeability of porous hollow-fiber membrane containing diethylamino groups on the grafted polymer branches. J. Memb. Sci., 71 (1-2), 1-12.

[67] Bishop P.L. and Yu T. (1999) A microelectrode study of redox potential change in biofilm. Wat. Sci. Technol. 39(7), 179-185.

[68] Casey E., Glennon B. and Hamer G. (1999b) Review of membrane aerated biofilm reactors. Resources, Conservation and Recycling 27, 203-215.

[69] Hibiya K., Tsuneda S. and Hirata A. (2000) Formation and characteristics of nitrifying biofilm on a membrane modified with positively-charged polymer chains. Colloids and Surfaces B: Biointerfaces 18(2), 105-112.

[70] Debus O. (1995) Transport and reaction of aromatics, O2 and CO2 within a membrane bound biofilm in competition with suspended biomass. Wat. Sci. Technol. 31(1), 129-141.

[71] Debus O., Baumgaerlt H. and Sekoulov I. (1994) Influence of fluid velocities on the degradation of volatile aromatic compounds in membrane bound biofilms. Wat. Sci. Technol. 29(10-11), 253-62.

[72] Wobus A. and Roske I. (2000) Reactors with membrane-grown biofilms: their capacity to cope with fluctuating inflow conditions and with shock loads of xenobiotics. Wat. Res. 34(1), 279-287.

[73] Casey E., Glennon B. and Hamer G. (1999a) Oxygen mass transfer characteristics in a membrane-aerated biofilm reactor. Biotechnol. Bioeng. 62(2), 183-192.

[74] Woolard C.R. and Irvine R.L. (1994) Biological treatment of hypersaline wastewater by a biofilm of halophilic bacteria. Wat. Environ. Res. 66, 230-235.

[75] Brindle K. and Stephenson T. (1996) The application of membrane biological reactors for the treatment of wastewaters. Biotechnol. Bioeng. 49, 601-610.

[76] Yamagiwa K., Yoshida M., Ito A. and Ohkawa A. (1998) A new oxygen supply method for simultaneous organic carbon removal and nitrification by a one-stage biofilm process. Wat. Sci. Technol. 37(4-5), 117-124.

[78] Amann R.I. (1995) In situ identification of microorganisms by whole cell hybridization with rRNA-targeted nucleic acid probes. In: Molecular microbial ecology manual 3.3.6. Kluwer Academic Publishers, Dordrecht, pp. 1-15.

[79] Mobarry B.K., Wagner M., Urbain V., Rittmann B.E. and Stahl D.A. (1996) Phylogenetic probe for analyzing abundance and spatial organization of nitrifying bacteria. Appl. Environ. Microbiol. 62, 2156- 2162.

[80] Suzuki Y., Hatano N., Ito S. and Ikeda H. (2000) Performance of nitrogen removal and biofilm structure of porous gas permeable membrane reactor. Wat. Sci. Technol. 41(4-5), 211-217.

[81] Tsuneda S., Endo T., Saito K., Sugita K., Horie K., Yamashita T. and Sugo T. (1998) Fluorescence study on the conformational change of an amino group-containing polymer chain grafted onto a polyethylene microfiltration membrane. Macromolecules 31(2), 366-370.

[82] Auresenia J., Morise T., Tsuneda S. and Hirata A. (1998). Reaction rate equations and kinetic parameters from batch experiments on three-phase fluidized bed biofilm reactor for wastewater treatment. Proceedings of the Regional Symposium on Chemical Engineering, Manila, Philippines, 31-38.

[83] Chen K.C., Lee S.C., Chin S.C. and Houng J.Y. (1998) Simultaneous carbon-nitrogen removal in wastewater using phosphorylated PVA-immobilized microorganisms. Enzyme and Microbial Technol. 23, 311-320.

[84] P. S. Stewart, A review of experimental measurements of effective diffusive permeabilities and effective diffusion coefficients in biofilms. Biotechnol. Bioeng. 59 (1998) 261-272.

[85] L. S. Fan, R. Leyva-Ramos, K. D. Wisecarver, B. J. Zehner, Diffusion of phenol through a biofilm growth on activated carbon particles in a draft tube three-phase fluidized

bed bioreactor, Biotechnol. Bioeng. 35 (1990) 279-286.
[86] M. Higa, A. Tanioka and K. Miyasaka, J. Mem. Sci. 49 (1990) 145.
[87] R. H. Perry and C. H. Chilton, Chemical Engineers Handbook, McGraw-Hill, New York, 1973
[88] N. Araki, K. Yazawa and H. Harada, J. Japan Society on Wat. Environ., 22 (1999) 600.
[89] M. Matsumura, T. Yamamoto, P. Wang, K. Shinabe and K. Yasuda, Wat. Res., 31 (1997) 102

# ACKNOWLEDGEMENT

## THANKS FOR YOUR HELPING

The present thesis is the collection of the studies, which have been carried out under the direction of Professor Akira Hirata, Associate Professor Satoshi Tsuneda (Department of Chemical engineering, Waseda University) as supervisors.

The author would like to express his gratitude to his supervisors: Professor Akira Hirata and Associate Professor Satoshi Tsuneda for giving him such a great chance to study, their helpful and useful advice and their encouragement throughout the study.

The author would like to appreciate Professor Kiyotaka Sakai, and Professor Izumi Hirasawa (Department of Chemical engineering, Waseda University) for their constructive and useful comments.

The author is very grateful to the all the members in the Hirata and Tsuneda Laboratory, especially to his group members: Mr. Joseph Auresenia, Mr. Jun Nagai, Mr. Akihiko Terada for their great help and contribution to carry out the study. The author also appreciates Ms. Yoko Ogawa secretary of the Laboratory for her heartful support.

The author was financially supported by a Research Fellow Ship for Young scientists, from Japan Society for the Promotion of Science (JSPS) since 2000 to 2002.

Finally, the author would like to express his deepest gratitude to his family for their continuous encouragement and support.

# ～　博士論文概要　～

湖沼や内湾の富栄養化現象は，生活排水や産業廃水に含まれる窒素化合物が流入するために起こる．この問題を未然に防ぐためには，これらの排水中から窒素化合物を高効率に除去する必要性がある．微生物による窒素除去は，低コストな排水処理技術として最もよく用いられている．しかしながら，硝化反応と脱窒反応という操作条件の全く異なる 2 つの反応を介さなければならないため，通常，複数の反応器が必要である．これに対して，小規模事業に導入可能な小型で維持管理の容易な単一槽型窒素除去システムの開発が強く望まれている．

本研究では，微生物が固体表面上に付着して形成する厚い細胞の層（生物膜と呼ばれる）に着目し，生物膜内の深さ方向の酸素濃度分布を制御することで単一槽内での窒素除去を実現できるシステムの開発に取り組んだ．開発を行う上で，生物膜内の酸素濃度分布や微生物生態分布を明らかにすることは重要であり，その手段として微小電極法および分子生物学的手法を活用した．微小電極は先端が非常に微小な針型センサであり，針の先端を生物膜に挿入することで生物膜内の特定の基質濃度分布を測定することができる．また，分子生物学的手法の一つである FISH（Fluorescence in situ hybridization）法を用いることで，培養操作を行うことなく生物膜内の微生物生態分布を観察できる．本研究では，これらの手法によって得られた生物膜内の物質移動および微生物生態学的知見を活かし，多孔質メンブレンの内側から酸素を供給するメンブレンエアレーション型バイオフィルムリアクタを考案した．そして，単一槽内で硝化反応と脱窒反応が逐次的に起こることを実証した，

本論文は 6 章より構成されている。以下に各章の概要を述べる．

第 1 章では，微小電極や各種顕微鏡，分子生物学的手法による生物膜内の現象解明に関する既往研究を整理し，また，本研究の背景である生物膜を用いた排水処理研究の動向をまとめた．それにより，本論文の意義，目的を述べた．

第 2 章では，酸素，アンモニア，硝酸，pH をターゲットとした微小電極の作成およびそれらを用いた生物膜内の各基質濃度分布の測定を行った．測定はそれぞれ高濃度に窒素成分を含む無機模擬排水または有機模擬排水が流入する完全混合型流動槽内から生物膜を取り出し，各基質濃度分布を追跡した．また，得られた基質濃度分布から速度パラメータを算出し，微生物反応速度を概算した．微小電極法が生物膜内の特定の基質濃度分布を測定するのに適したツールであることが示された．

第 3 章では，微小電極を用いて測定した生物膜内の酸素濃度分布およびその結果を用いて算出した速度パラメータを基に，さまざまな生物膜厚み，生物膜密度およびバルク酸素濃度における生物膜内の酸素濃度分布をシミュレートした．シミュレーションは，微生物反応項として Monod 型を用い，有限要素法により非線形反応式を解くことで行った．その結果によると，生物膜厚みが増すことによって，生物膜の中心部（バルクから遠い部位）では酸素の少ない状態，もしくは無酸素状態の部

位が形成されることがわかった．また，これらの部位では，還元反応である脱窒反応が起きていることが水質測定からも推測された．これにより，生物膜厚みや酸素の供給速度を制御することによって生物膜内に局所的に異なった反応場を作ることが可能であり，異なった微小環境反応場を利用することで単一槽内，単一生物膜内において硝化・脱窒同時反応が可能であることがわかった．また，排水処理プロセスのさまざまな状況に応じて生物膜の厚み，密度および微生物生態系を制御する必要があり，それらの制御において酸素の供給速度が果たす役割は非常に大きいことが示された．

第４章では，流入排水の負荷変動時，特に濃度変動時における生物膜内酸素濃度の変化を追った．これにより，負荷変動時の排水処理における生物反応の特異現象の解明に努めた．負荷変動は急激に流入排水濃度を上げるステップアップ実験と濃度を下げるステップダウン実験を行った．その結果，生物膜内の酸素濃度分布はその瞬間のバルクの酸素濃度分布に大きく依存することがわかった．また，ほとんどの硝化細菌は生物膜内に存在し，その硝化反応速度は生物膜内の酸素濃度に大きく依存することがわかった．以上の結果から，生物膜内に適切に硝化細菌を保持し，生物膜へ酸素を十分に供給すれば硝化反応がスムーズに進行し，さらに生物膜内に酸素濃度の低い部位が存在すればそこで脱窒反応が逐次的に起こることが示唆された．一方，バルクの酸素濃度が低い状態，つまり生物膜へ酸素がほとんど供給されない状態では，硝化反応が起きず，硝化律速となるため窒素除去はできなくなることも同時に示された．

第５章では，多孔質担体の中空糸状メンブレンを支持体として用い，その外側に有用微生物（硝化細菌）を付着させ，内側から酸素を供給する“メンブレンエアレーション型バイオフィルムリアクタ（Membrane Aeration Biofilm Reactor; MABR）”を作製し，実験室規模での実証試験を行った．開発に当たり，まずメンブレンに効率よく硝化細菌を付着させる工夫を行った．一般に中性 pH 域では微生物細胞の表面がマイナスに帯電していることを踏まえ，本研究では，グラフト重合法によりメンブレン表面にジエチルアミノ基を導入してプラスに帯電させた．その結果，メンブレン表面上に硝化細菌を短時間で効率よく付着させることが可能になった．つぎに，グラフト重合処理を行った中空糸状メンブレンを用いて MABR を作製し，人工下水の処理試験を行った．その結果，排水流入開始 50 日後に 95%以上の窒素除去率を達成し，単一槽での硝化・脱窒反応を実現した．また，この MABR では排水中の炭素成分も同時に除去でき，炭素・窒素同時除去を可能にした．それぞれの処理速度は炭素成分については 0.42 kg-C/($m^3$・day)，窒素成分については 0.16 kg-N/($m^3$・day)であった．さらに，運転中に得られた生物膜に対して微小電極を用いて生物膜内の深さ方向の pH，$NH_4^+$，$NO_3^-$濃度分布を測定したところ，$NH_4^+$は反応器下部から中部において除去されており，$NO_3^-$は反応器全体でほとんど確認されなかった．さらに，反応器内の生物膜および浮遊汚泥に対して FISH 法を適用し，アンモニア酸化細菌およびその他の真正細菌について生息場所を特定した結果，アンモニア酸化細菌は主に生物膜内に広く分布しており，その他の細菌（脱窒細菌を含む）は主に生物膜外の沈降汚泥や浮遊汚泥中に分布していることが判明した．

第６章では，本論文の総括および展望を記述した．

以上，本研究では窒素除去プロセスにおける生物膜内の物理現象や生態分布の解析を行った．特に，生物膜内の酸素濃度分布に注目し，さまざまな厚みをもつ生物膜に対して酸素濃度分布を測定し，シミュレーションを行った．また得られた知見を応用し，生物膜内での微小環境を制御することで単一槽内での硝化・脱窒同時反応を行うことができるメンブレンエアレーション型バイオフィルムリアクタを開発した．これらの研究成果は窒素除去プロセスの効率化のみならず微生物反応工学および環境浄化技術の発展に大いに寄与するものと期待される．